

# Microbiome analysis of 940 lung cancers in never-smokers reveals lack of clinically relevant associations

Received: 29 May 2025

Accepted: 14 November 2025

Cite this article as: McElderry, J.P., Zhang, T., Zhao, W. *et al.* Microbiome analysis of 940 lung cancers in never-smokers reveals lack of clinically relevant associations. *Nat Commun* (2025). <https://doi.org/10.1038/s41467-025-66780-y>

John P. McElderry, Tongwu Zhang, Wei Zhao, Phuc H. Hoang, Samuel Anyaso-Samuel, Jian Sang, Azhar Khandekar, Caleb Hartman, Frank J. Colón-Matos, Mona Miraftab, Monjoy Saha, Olivia Lee, Sunandini Sharma, Kristine M. Jones, Bin Zhu, Marcos Diaz-Gay, Luis Mas, Oscar Gerardo Arrieta Rodriguez, Eric S. Edell, Jacobo Martínez Santamaría, Matthew B. Schabath, Sai Yendamuri, Marta Manczuk, Jolanta Lissowska, Beata Świątkowska, Anush Mukeria, Oxana Shangina, David Zaridze, Ivana Holcatova, Vladimir Janout, Dana Mates, Simona Ognjanovic, Milan Savic, Milica Kontic, Yohan Bossé, Bonnie E. Gould Rothberg, David C. Christiani, Valerie Gaborieau, Paul Brennan, Geoffrey Liu, Paul Hofman, Maria Pik Wong, Kin Chung Leung, Chih-Yi Chen, Chao Agnes Hsiung, Nathaniel Rothman, Charles Leduc, Marina K. Baine, William D. Travis, Lynette M. Sholl, Philippe Joubert, Robert Homer, Soo-Ryun Yang, Qing Lan, Martin A. Nowak, David C. Wedge, Ludmil B. Alexandrov, Stephen J. Chanock, Emily Vogtmann, Christian C. Abnet, Jianxin Shi & Maria Teresa Landi

We are providing an unedited version of this manuscript to give early access to its findings. Before final publication, the manuscript will undergo further editing. Please note there may be errors present which affect the content, and all legal disclaimers apply.

If this paper is publishing under a Transparent Peer Review model then Peer Review reports will publish with the final article.

1 **Microbiome analysis of 940 lung cancers in never-smokers reveals lack of clinically relevant**  
2 **associations**

3  
4 John P. McElderry<sup>1</sup>, Tongwu Zhang<sup>1</sup>, Wei Zhao<sup>1</sup>, Phuc H. Hoang<sup>1</sup>, Samuel Anyaso-Samuel<sup>1</sup>, Jian  
5 Sang<sup>1</sup>, Azhar Khandekar<sup>1,2</sup>, Caleb Hartman<sup>1</sup>, Frank J. Colón-Matos<sup>1</sup>, Mona Miraftab<sup>1</sup>, Monjoy  
6 Saha<sup>1</sup>, Olivia Lee<sup>1</sup>, Sunandini Sharma<sup>1</sup>, Kristine M. Jones<sup>1,3</sup>, Bin Zhu<sup>1</sup>, Marcos Díaz-Gay<sup>2</sup>, Luis  
7 Mas<sup>4</sup>, Oscar Gerardo Arrieta Rodriguez<sup>5</sup>, Eric S. Edell<sup>6</sup>, Jacobo Martínez Santamaría<sup>7</sup>, Matthew  
8 B. Schabath<sup>8</sup>, Sai Yendumuri<sup>9</sup>, Marta Manczuk<sup>10</sup>, Jolanta Lissowska<sup>10</sup>, Beata Świątkowska<sup>11</sup>,  
9 Anush Mukeria<sup>12</sup>, Oxana Shangina<sup>12</sup>, David Zaridze<sup>12</sup>, Ivana Holcatova<sup>13,14</sup>, Vladimir Janout<sup>15</sup>,  
10 Dana Mates<sup>16</sup>, Simona Ognjanovic<sup>17</sup>, Milan Savic<sup>18</sup>, Milica Kontic<sup>19</sup>, Yohan Bossé<sup>20</sup>, Bonnie E.  
11 Gould Rothberg<sup>21</sup>, David C. Christiani<sup>22,23</sup>, Valerie Gaborieau<sup>24</sup>, Paul Brennan<sup>24</sup>, Geoffrey Liu<sup>25</sup>,  
12 Paul Hofman<sup>26</sup>, Maria Pik Wong<sup>27</sup>, Kin Chung Leung<sup>28</sup>, Chih-Yi Chen<sup>29,30</sup>, Chao Agnes Hsiung<sup>31</sup>,  
13 Nathaniel Rothman<sup>1</sup>, Charles Leduc<sup>32</sup>, Marina K. Baine<sup>33</sup>, William D. Travis<sup>33</sup>, Lynette M. Sholl<sup>34</sup>,  
14 Philippe Joubert<sup>20</sup>, Robert Homer<sup>35</sup>, Soo-Ryun Yang<sup>33</sup>, Qing Lan<sup>1</sup>, Martin A. Nowak<sup>36,37</sup>, David C.  
15 Wedge<sup>38</sup>, Ludmil B. Alexandrov<sup>2</sup>, Stephen J. Chanock<sup>1</sup>, Emily Vogtmann<sup>1</sup>, Christian C. Abnet<sup>1</sup>,  
16 Jianxin Shi<sup>1</sup>, Maria Teresa Landi<sup>1,\*</sup>

17  
18 \* Correspondence should be directed to [landim@nih.gov](mailto:landim@nih.gov)

19  
20 <sup>1</sup>Division of Cancer Epidemiology and Genetics, National Cancer Institute, Bethesda, Maryland,  
21 United States of America

22 <sup>2</sup>Department of Cellular and Molecular Medicine and Department of Bioengineering and  
23 Moores Cancer Center, UC San Diego, La Jolla, California, United States of America

24 <sup>3</sup>Cancer Genomics Research Laboratory, Leidos Biomedical Research, Frederick National  
25 Laboratory for Cancer Research, Frederick, Maryland, United States of America

26 <sup>4</sup>Medical Oncology Unit, Instituto Nacional de Enfermedades Neoplásicas (INEN), Lima, Peru

27 <sup>5</sup>Thoracic Oncology Unit, Instituto Nacional de Cardiología (INCan), Mexico City, México

28 <sup>6</sup>Division of Pulmonary and Critical Care Medicine, Mayo Clinic, Rochester, Minnesota, United  
29 States of America

30 <sup>7</sup>Biobanco IBSP-CV FISABIO; Red Valenciana de Biobancos, Cataluña, Valencia, Spain

31 <sup>8</sup>Department of Cancer Epidemiology, H. Lee Moffitt Cancer Center and Research Institute,  
32 Tampa, Florida, United States of America

33 <sup>9</sup>Thoracic Surgery, Roswell Park Comprehensive Cancer Center, Buffalo, New York, United  
34 States of America

35 <sup>10</sup>Department of Cancer Epidemiology and Primary Prevention, Maria Skłodowska-Curie  
36 National Research Institute of Oncology, Warsaw, Poland

37 <sup>11</sup>Department of Environmental Epidemiology, Nofer Institute of Occupational Medicine, Łódź,  
38 Poland

39 <sup>12</sup>Department of Clinical Epidemiology, N.N. Blokhin National Medical Research Centre of  
40 Oncology, Moscow, Russia

41 <sup>13</sup>Institute of Public Health & Preventive Medicine, 2nd Faculty of Medicine, Charles University,  
42 Prague, Czech Republic

43 <sup>14</sup>Department of Oncology, 2nd Faculty of Medicine, Charles University and Motol University  
44 Hospital, Prague, Czech Republic

45 <sup>15</sup>Faculty of Health Sciences, Palacky University, Olomouc, Czech Republic  
46 <sup>16</sup>Department of Occupational Health and Toxicology, National Center for Environmental Risk  
47 Monitoring, National Institute of Public Health, Bucharest, Romania  
48 <sup>17</sup>International Organization for Cancer Prevention and Research (IOCPRI), Belgrade, Serbia  
49 <sup>18</sup>Department of Thoracic Surgery, Clinical Center of Serbia, Belgrade, Serbia  
50 <sup>19</sup>Clinic of Pulmonology, Clinical Center of Serbia, Belgrade, Serbia  
51 <sup>20</sup>Institut universitaire de cardiologie et de pneumologie de Québec, Laval University, Quebec  
52 City, Canada  
53 <sup>21</sup>UMMG Dept of Medicine - Hospital Medicine, Miller School of Medicine, Medical Campus,  
54 University of Miami, Miami, Florida, United States of America  
55 <sup>22</sup>Department of Environmental Health, Harvard T.H. Chan School of Public Health, Boston,  
56 Massachusetts, United States of America  
57 <sup>23</sup>Department of Medicine, Massachusetts General Hospital, Boston, Massachusetts, United  
58 States of America  
59 <sup>24</sup>Genomic Epidemiology Branch, International Agency for Research on Cancer (IARC/WHO),  
60 Lyon, France  
61 <sup>25</sup>Division of Medical Oncology, Medicine, Princess Margaret Cancer Centre, Temerty Faculty of  
62 Medicine, Dalla Lana School of Public Health, University of Toronto, Toronto, Ontario, Canada  
63 <sup>26</sup>Nice University Hospital Centre (Nice UHC) - University Côte d'Azur and the Nice Biobank CRB,  
64 Nice, France  
65 <sup>27</sup>Queen Mary Hospital, The University of Hong Kong, Hong Kong, China  
66 <sup>28</sup>Department of Pathology, The University of Hong Kong, Hong Kong, China  
67 <sup>29</sup>Institute of Medicine, Chung Shan Medical University, Taichung, Taiwan  
68 <sup>30</sup>Division of Thoracic Surgery, Department of Surgery, Chung Shan Medical University Hospital,  
69 Taichung, Taiwan  
70 <sup>31</sup>Institute of Population Health Sciences, National Health Research Institutes, Zhunan, Taiwan  
71 <sup>32</sup>Department of Pathology, Centre Hospitalier de l'Université de Montréal, Montreal, Canada  
72 <sup>33</sup>Department of Pathology and Laboratory Medicine, Memorial Sloan Kettering Cancer Center,  
73 New York, New York, United States of America  
74 <sup>34</sup>Department of Pathology, Brigham and Women's Hospital, Boston, Massachusetts, United  
75 States of America  
76 <sup>35</sup>Department of Pathology, Yale School of Medicine, New Haven, Connecticut, United States of  
77 America  
78 <sup>36</sup>Department of Mathematics, Harvard University, Cambridge, Massachusetts, United States of  
79 America  
80 <sup>37</sup>Department of Organismic and Evolutionary Biology, Harvard University, Cambridge,  
81 Massachusetts, United States of America  
82 <sup>38</sup>Manchester Cancer Research Centre, Division of Cancer Sciences, University of Manchester,  
83 Manchester, United Kingdom  
84

85 **Abstract**

86

87 In spite of the growing interest in the microbiome in human cancer, there are currently only  
88 small-scale lung cancer microbiome studies conducted directly on tissue. As part of the  
89 *Sherlock-Lung* study, we studied the microbiomes of 940 lung cancers (4,090 samples) in never  
90 smokers (LCINS) directly from lung tissue using three data types: 16S rRNA gene sequencing  
91 (16S), whole-genome sequencing (WGS) with paired blood, and RNA-seq. We observe very low  
92 biomass and few microbiome associations in LCINS using 16S and WGS tissue. Using RNA-seq,  
93 we observe more total microbial reads, and decreased relative abundance of several  
94 commensal bacteria at the genus and species levels in tumors relative to paired normal lung  
95 tissue. Among all datasets, we see no consistent associations between the lung tissue  
96 microbiome, or circulating bacterial DNA, and any available demographic and clinical features,  
97 including age, sex, genetic ancestry, second-hand tobacco smoking exposure, LCINS histology,  
98 stage, and overall survival. We also observe no microbiome associations with any human  
99 genomic alterations within the same samples. Every null result should be interpreted with  
100 caution given the possibility of future methodological breakthroughs. However, all together,  
101 using multiple data types in nearly 1,000 patients, we find no substantive role for the lung  
102 cancer microbiome in treatment-naïve LCINS.

103 **INTRODUCTION**

104

105 The human cancer microbiome is a rapidly growing field of research. To date, most major  
106 studies on the human cancer microbiome have focused on organs with high bacterial  
107 abundance, e.g., mouth, stomach, and colon, identifying connections between the microbiome  
108 and cancer incidence or progression. Additionally, several specific microbes have been shown  
109 to produce genotoxins, suggesting a possible role in cancer initiation. These include  
110 *Helicobacter pylori*, a Group 1 carcinogen which causes stomach cancer<sup>1</sup>, as well as pks+  
111 *Escherichia coli*<sup>2-10</sup>, *Bacteroides fragilis*<sup>11-15</sup>, and *Fusobacterium nucleatum*<sup>16-22</sup>, each associated  
112 with colorectal cancer. Resultantly, enthusiasm for the microbiome as a target for cancer early  
113 detection<sup>23-25</sup>, prevention, and treatment<sup>26</sup> has grown significantly in recent years. Despite this,  
114 research on the cancer microbiomes of most organs has been limited, including on the lung.

115

116 Relatively little is known about the lung microbiome even in healthy individuals. Historically, the  
117 lungs have been considered sterile organs due to repeated failure to culture bacteria from lung  
118 samples<sup>27</sup>. This idea has since been challenged using culture-free sequencing methods. Much of  
119 the current research on the lung microbiome is derived from samples collected via sputum or  
120 bronchoalveolar lavage (BAL). Studies performed on healthy individuals and cancer patients  
121 with samples collected using BAL have characterized the lung microbiome as being similar in  
122 composition to the oral and upper airway microbiomes, albeit at much lower total  
123 abundance<sup>28-32</sup>. In contrast, small-scale studies conducted on surgically removed tumor and  
124 normal lung tissue - which theoretically precludes contamination from the upper airways<sup>33</sup> -  
125 identified much lower proportions of upper airway bacteria<sup>34-38</sup>. A recent study of the murine  
126 lung microbiome concluded that although both methods may be valid for studying the lung  
127 microbiome, samples collected from BAL fluid versus directly from lung tissue within the same  
128 animals can be distinguished *via* beta diversity analysis<sup>39</sup>.

129

130 Alterations in the lung microbiome are connected with several diseases<sup>40</sup> such as chronic  
131 obstructive pulmonary disease<sup>41-44</sup>, asthma<sup>45-47</sup>, and idiopathic pulmonary fibrosis<sup>48</sup>.  
132 Furthermore, changes in the lung microbiome of mice has been shown to influence  
133 development of multiple sclerosis in the brain<sup>49</sup>. Many studies have also identified differences  
134 in the lung microbiomes of healthy versus cancer patients<sup>32,36-38,50-54</sup> and tumor versus adjacent  
135 normal tissue<sup>34,36-38</sup>, and several have found associations with tumor clinical features, such as  
136 histology<sup>55</sup>, stage<sup>34</sup>, and progression<sup>56</sup>. However, these studies are predominantly based on  
137 small sets of patients (on average less than 100 subjects, ranging from 10<sup>51</sup> to 176<sup>37</sup> subjects  
138 total), resulting in discrepant results. Additionally, most datasets are composed primarily of  
139 smokers, and thus the role of the microbiome specifically in never-smoker lung cancer is largely  
140 unstudied.

141

142 In this study, we used 16S sequencing to analyze the microbiome of 701 surgically removed  
143 treatment-naive lung cancers in never smokers (LCINS) plus 563 tumor-adjacent normal lung  
144 samples, the largest sample collection to date. To further increase the size of our study, we  
145 leveraged an additional 1,623 WGS samples (tumor, normal lung, blood) and 1,203 RNA-seq  
146 samples (tumor, normal lung) collected as part of Sherlock-Lung and investigated bacterial

147 reads in these samples. With considerable overlap of subjects between datasets, this study  
148 includes a total of 4,090 samples from 940 cancer patients who were treatment naive at the  
149 time of sample collection. Despite the comprehensive analysis, we found no evidence for  
150 clinically-relevant associations between the composition or diversity of the lung cancer  
151 microbiome and LCINS demographics, tumor characteristics, previous respiratory diseases,  
152 genomic features, and survival or recurrence.

153

## 154 RESULTS

155

### 156 Description of study samples

157

158 This study is based on the *Sherlock-Lung* project<sup>57</sup> of LCINS. Briefly, as part of *Sherlock-Lung*  
159 (hereafter referred to simply as *Sherlock*), we have analyzed WGS<sup>58,59</sup>, 16S, and RNA-seq data  
160 from hundreds of LCINS across North and South America, Europe, and Asia, together with  
161 epidemiological, clinical, and morphological features.

162

163 Specifically, we examined the microbiomes of 940 LCINS patients, 740 females and 200 males of  
164 median age 64.7 years, with 639 paired adjacent normal tissue plus 447 WGS blood samples  
165 (Table 1, Supplementary Data 1). Sex was self-reported and confirmed via WGS where available.  
166 Based on WGS-derived genetic ancestry, this cohort includes 441 patients of European ancestry  
167 from the United States, Canada, and Europe; 338 of East Asian ancestry from Hong Kong,  
168 Taiwan, the United States, and Canada; 28 of Native American/Mixed ancestry from Europe and  
169 Canada, plus four of African ancestry from the United States and Canada (Table 1,  
170 Supplementary Data 1). For patients without WGS data, ancestry was self-reported, including  
171 58 patients of East Asian ancestry from Hong Kong, Taiwan, and Canada; 46 of European  
172 ancestry from Europe and the United States; and 24 of Native American/Mixed ancestry (Table  
173 1, Supplementary Data 1). One patient from Canada was of unknown ancestry.

174

175 As is typical in LCINS, the most common histology was adenocarcinomas ( $n=811$ ), followed by  
176 carcinoid tumors ( $n=60$ ), squamous cell carcinomas ( $n=40$ ), and various other tumor types  
177 ( $n=29$ ) (Table 1, Supplementary Data 1). The majority of tumors ( $n=522$ ) and normal lung tissue  
178 ( $n=278$ ) were sequenced using all three approaches: WGS, 16S, and RNA-seq (Figure 1a,  
179 Supplementary Data 1).

180

### 181 Multi-omic identification of bacterial reads

182

183 Recently, debate has emerged about best practices for microbiome research<sup>23,60–62</sup> using next-  
184 generation sequencing (NGS) after several methodological errors were identified in a major  
185 pan-cancer study on the cancer microbiome<sup>60</sup>. These errors resulted in millions of unaligned  
186 human sequences being mis-identified as bacterial, which affected some of the findings of the  
187 original paper<sup>62</sup>. To avoid assigning human reads to bacterial genomes, as discussed in Gihawi  
188 et al.<sup>61</sup>, we aligned all reads to the CHM13 T2T genome<sup>63</sup> to filter out as many human  
189 sequences as possible prior to taxonomic assignment with Kraken2<sup>64</sup> (Figure 1b), then extracted  
190 unaligned reads from this re-alignment for use with Kraken2. Following taxonomic assignment,

191 we used Bracken<sup>65</sup> to adjust read counts at the genus level for both WGS and 16S sequencing,  
192 but chose not to use Bracken for the RNA-seq dataset as Bracken was developed for DNA-based  
193 sequencing (Methods). Taxonomic assignment results are presented in Supplementary Data 2-  
194 4.

195  
196 Despite rigorous filtering to remove human reads, many unaligned reads in all datasets were  
197 assigned by Kraken2 to the human genome (median 48.1%, 6.4%, 8.3% in RNA-seq, WGS, 16S  
198 respectively) (Figure 1c, Supplementary Data 2-4). These reads likely originate from imperfect  
199 mapping of human<sup>61</sup>, often repetitive, reads to the human genome. In 16S samples, many  
200 human reads originate from the mitochondrial genome which contains a 16S rRNA gene that  
201 may be amplified off-target in 16S experiments<sup>66</sup>. RNA-seq samples contained the most human  
202 reads after alignment, perhaps in part due to the relative difficulty of filtering spliced human  
203 RNA sequences via mapping.

204  
205 Many reads were of unknown origin (median 4.9%, 86.7%, 55.0% in RNA-seq, WGS, 16S,  
206 respectively), likely originating from sequencing artifacts, short sequences that could not be  
207 confidently assigned, or reads from microbes with incomplete reference genomes. Almost all  
208 taxonomically assigned, non-human reads were bacterial (median 99.9%, 98.7%, 100% among  
209 non-human reads in RNA, WGS, 16S, respectively), thus we focused our downstream analyses  
210 solely on the bacterial component of the datasets.

211  
212 We next generated two datasets from the bacterial abundances: one with batch correction  
213 applied using ComBat-Seq, and one without batch correction. Reads without batch correction  
214 were used solely to describe the landscape of the lung cancer microbiome as batch correction  
215 can, in some cases, greatly inflate the abundances of rare bacteria<sup>61</sup>. Batch corrected data was  
216 used for all statistical associations between the microbiome and clinical or demographic  
217 features. WGS associations were performed separately for samples sequenced for this study  
218 ( $n=1,246$ ) and samples from our previous study ( $n= 377$ , Zhang et al. 2021)<sup>58</sup> to account for a  
219 strong batch effect (Supplementary Figure 1). Results from these two WGS data subsets were  
220 analyzed separately and combined as a meta-analysis downstream. For 16S data, abundances  
221 were not batch corrected as these samples did not show evidence of strong batch effects.

222  
223 Both batch corrected and uncorrected abundances were then decontaminated *in silico*. For 16S  
224 samples, PCR negative controls were used to calculate bacterial contamination fractions with  
225 the SCRUB<sup>67</sup> algorithm, using PCR well location information to track well-to-well leakage. The  
226 WGS and RNA-seq datasets were originally collected for studies on human  
227 genomics/transcriptomics and therefore did not have paired negative controls, as this is not  
228 standard for non-metagenomic experiments. Despite this limitation, we sought to include both  
229 datasets as complementary data together with our 16S dataset to corroborate any findings. In  
230 all datasets, we performed literature-based decontamination by removing bacterial genera that  
231 are found to frequently contaminate NGS experiments<sup>68</sup> and have not been known to colonize  
232 human microbiomes<sup>69</sup>(Methods). Removal of reads at the genus level were recursively  
233 propagated<sup>70</sup> to higher taxonomic ranks to remove contamination at all levels of the taxonomy.

234

235 The raw composition of the microbiome at the phylum and genus levels are shown in  
236 Supplementary Figure 2a. Prior to decontamination, we observed minimal correlation between  
237 sequencing platforms within the same samples (Supplementary Figure 2c-f). Following batch  
238 correction and decontamination, phylum-level relative abundances and genus-level Shannon  
239 alpha diversity were significantly, but weakly, correlated across all datasets (alpha diversity  
240 Pearson R values between 0.15-0.33, phylum-level abundances Pearson R values between 0.0-  
241 0.27) (Supplementary Figure 3). Furthermore, within-subject beta diversity accounted for a high  
242 percentage of overall variance among all samples (Permutational Multivariate ANOVA, 999  
243 iterations,  $p=0.001$ ,  $R^2=0.455$ ; Supplementary Data 5). This indicates that although microbiome  
244 composition and diversity results differ across sequencing modalities, the microbiome  
245 composition per subject, relative to other subjects, is similar across datasets.  
246

#### 247 **The lung cancer microbiome has low biomass across all data types**

248  
249 16S samples had the most bacterial reads per million, as expected due to the targeted nature of  
250 16S rRNA sequencing, followed by RNA-seq, and lastly WGS (Figure 1d). After read filtering to  
251 remove contaminants, we observed low absolute bacterial read totals in WGS (median 344,  
252 162, and 1,440 bacterial reads in tumor, adjacent lung, and blood samples, respectively) and  
253 16S sequencing samples (median 730 and 773 bacterial reads in tumor and adjacent normal  
254 tissue, respectively). The median numbers of bacterial reads in RNA-seq samples were 9,080  
255 and 11,053 in tumor and adjacent normal samples, respectively (Figure 1e). Of note, WGS  
256 samples were sequenced to differing depth between tumor (median human genome coverage  
257 87X) and normal lung tissue (median coverage 34x, read depth statistics for all samples  
258 provided in Table 2). We did not use microbiome data from WGS for alpha or beta diversity  
259 comparisons between tumor and normal lung tissue due to this difference, which could bias the  
260 results, and also due to the extremely low bacterial read depth in normal tissue.  
261

262 To put these results into context, we compared the read counts of Sherlock WGS samples with  
263 those from the Pan-cancer analysis of whole genomes working group (PCAWG)<sup>71</sup> (Figure 1f). We  
264 used the read counts from the PCAWG breast (BRCA), bladder (BLCA), and head and neck  
265 squamous cell carcinoma (HNSC) WGS samples re-analyzed by Gihawi et al<sup>61</sup>, and re-analyzed  
266 the PCAWG lung cancer WGS ( $n=96$ , of which 81 from smokers, not reported in Gihawi et al<sup>61</sup>).  
267 16S samples were not included in this comparison as no public 16S data both derived from lung  
268 tissue and including total read counts information were available. We found that Sherlock WGS  
269 samples had lower genus-level bacterial reads in comparison to lung and other cancer types.  
270 Differences in DNA extraction and sequencing as well as the different smoking status may  
271 contribute to these findings as PCAWG WGS is known to have batch-dependent bacterial  
272 contamination<sup>72</sup> (Figure 1f).  
273

274 For downstream statistical tests, RNA-seq samples with less than 500 reads were excluded to  
275 improve the reliability of associations. Due to the considerably lower read depth of 16S and  
276 WGS samples, this read cutoff was relaxed to 250 reads in 16S and 100 reads in WGS to  
277 preserve sample size. For intra-class correlation analyses (phylum-level relative abundances,

278 alpha diversity, beta diversity), a cutoff of 250 reads was applied to all datasets to allow for  
279 valid comparisons.

280

## 281 Microbiome composition across tissue and data types

282

283 *Proteobacteria* (also known as *Pseudomonadota*, mean relative abundances per sequencing  
284 modality ranging 36.4 - 67.4%), *Actinobacteria* (also known as *Actinomycetota*, mean relative  
285 abundances 15.0 - 21.0%), and *Firmicutes* (also known as *Bacillota*, mean relative abundances  
286 14.5 - 31.1%), were the most abundant phyla across all Sherlock datasets and biospecimen  
287 types (Figure 2a). However, their mean relative abundances, particularly that of *Firmicutes*,  
288 varied substantially across sequencing modalities (Figure 2b). Several bacterial genera were  
289 observed across all three datasets, e.g., *Acinetobacter* (mean relative abundance 5.9 - 8.6%),  
290 *Corynebacterium* (12.9 - 13.2%), *Pseudomonas* (2.7 – 23.9%), *Staphylococcus* (3.5 - 11.1%), and  
291 *Streptococcus* (2.3 – 3.9%; Figure 2c, Supplementary Figure 4). Notably, these were all among  
292 the top ten most abundant bacterial genera in a recent 16S sequencing study of 245 lung  
293 tumors (43 never smokers)<sup>35</sup> with many negative controls and strict decontamination, thus  
294 demonstrating a degree of concordance between studies.

295

296 Among the three datasets, RNA-seq samples had the highest genus richness of all datasets  
297 regardless of read sampling depth (Figure 2d).

298

299 Comparing the tumor versus normal lung microbiome in 16S data, we identified few  
300 differentially abundant bacteria which were not significant after multiple testing correction  
301 (Figure 3a, Supplementary Figure 5a, Supplementary Data 6), and observed slightly decreased  
302 alpha diversity in tumor samples (mean diversity=1.9) compared to paired normal tissues  
303 (mean diversity=2.0, Wilcoxon  $p=0.0015$ , Figure 3b). Using RNA-seq, several bacterial genera  
304 were enriched in normal tissue compared with tumors (Figure 3c, Supplementary Figure 5b,  
305 Supplementary Data 7), and sample alpha diversity was marginally decreased in tumor tissue  
306 relative to paired normal tissues (Wilcoxon  $p=0.028$ , mean diversity in tumors=3.03, normal  
307 tissue=3.08) (Figure 3d). Again using RNA-seq, we obtained similar results when we tested  
308 differential abundance of species within the most abundant genera (*Acinetobacter*,  
309 *Corynebacterium*, *Pseudomonas*, *Staphylococcus*, and *Streptococcus*): many *Corynebacterium*  
310 and *Staphylococcus* species were significantly enriched in normal lung tissue versus tumor  
311 tissue, and several species of *Pseudomonas* and *Acinetobacter* were marginally enriched in  
312 tumor tissue versus normal lung tissue when analyzed using ANCOM-BC (Supplementary Figure  
313 5c,d, Supplementary Data 8).

314

315 We performed power calculations to derive the minimum effect sizes achieving 80% statistical  
316 power for detecting tumor/normal differences using either Bonferroni corrected p-value  
317 threshold or using 0.01 as p-value threshold (Methods). For tumor-normal comparisons, the  
318 minimum effect sizes are calculated as  $\beta = 0.14$  for RNA-seq analysis ( $\beta = 3.9\beta - 5$ , Bonferroni  
319 correction, 1279 taxa) or  $\beta = 0.096$  ( $\beta = 0.01$ ), and  $\beta = 0.23$  for 16S sRNA analysis ( $\beta = 2.8\beta -$   
320 4, Bonferroni correction, 141 taxa) or  $\beta = 0.17$  ( $\beta = 0.01$ ). This suggests that we have sufficient

321 statistical power to detect tumor-normal differences in the microbiome with modest effect  
322 sizes if they were present in our data.

323  
324 We did not compare tumor WGS data with normal lung tissue WGS because of the different  
325 read depth between tumor and normal tissue, as previously stated.  
326

### 327 **Microbiome characteristics in relation to demographic and clinical factors**

328  
329 We tested several factors in association with microbiome features. First, we examined the  
330 relationship between microbiome alpha diversity versus clinical and demographic features. We  
331 observed variation in richness (Kruskal-Wallis,  $p<2.2e-16$ ) and diversity (Kruskal-Wallis,  
332  $p=0.00033$ ) between study sites (Supplementary Figure 6a,b). Other associations in all datasets  
333 were not significant after multiple testing corrections (Figure 3e). Some associations were  
334 nominally significant. In WGS, stage IV tumors had increased genus richness relative to Stage I  
335 tumors (unadjusted  $p=0.05$ ,  $\beta=1.14$ , 95% confidence interval= [-0.509, 2.79]), and carcinoid  
336 tumors had decreased alpha diversity compared to adenocarcinomas ( $\beta= -0.21$ , unadjusted  
337  $p=0.02$ , 95% confidence interval= [-0.36, -0.06]). In the 16S dataset, Native American/mixed  
338 ancestry patients had decreased tumor alpha diversity relative to European patients  
339 (unadjusted  $p=0.03$ ,  $\beta= -0.26$ , 95% confidence interval= [-0.50, -0.02]).  
340

341 Measuring beta diversity, WGS and 16S datasets showed significant variation according to  
342 sample study site while RNA-seq after batch correction was not significantly associated. The  
343 RNA-seq dataset showed small, significant differences according to tumor-normal status, age at  
344 diagnosis, histology, and vital status, but no differences were observed according to ancestry,  
345 sex, tumor stage, or development of metastases. No clinical and demographic variables were  
346 associated with beta-diversity using 16S or WGS data (Supplementary Figure 6c).  
347

348 Recent research has suggested that circulating bacterial DNA in blood may be associated with  
349 clinical outcomes, including in lung cancer<sup>23-25</sup>. To investigate this hypothesis, we tested  
350 associations between blood microbial diversity measures and lung cancer clinical features. We  
351 correlated relative abundances between paired tumor and blood samples at the phylum level  
352 to test the plausibility of detecting lung bacteria in blood samples. Among the most prevalent  
353 phyla (*Proteobacteria*, *Actinobacteria*, *Firmicutes*, and *Bacteroidetes*), only abundance of  
354 phylum *Firmicutes* ( $p<2.2e-16$ , Pearson  $R=0.5$ ) and *Proteobacteria* ( $p=9.1e-05$ , Pearson  $R=0.19$ )  
355 was significantly correlated between tumor and paired blood samples (Supplementary Figure  
356 7a). At the genus level, abundance of *Staphylococcus* (classified under phylum *Firmicutes*) was  
357 correlated between blood and tumor samples ( $p<2.2e-16$ , Pearson  $R=0.58$ ). Genus richness and  
358 alpha diversity in blood samples were not associated with any tested clinical features, including  
359 lung cancer stage, histology, risk of recurrence, or vital status (Supplementary Figure 7b), and  
360 beta diversity in blood was associated with sample study sites and weakly associated with vital  
361 status ( $p=0.026$ ,  $R^2=0.008$ ) and tumor stage ( $p=0.043$ ,  $R^2=0.02$ ) (Supplementary Figure 7c).  
362

363 Notably, using RNA-seq, 16S, and tumor and blood WGS data, we found no associations  
364 between genus-level relative abundances for any bacteria, adjusted by histology and age in ten

365 year categories, and overall survival, stratified by study site, age at diagnosis (age>65, age≤65),  
366 and tumor stage (Figure 4). Similarly, no significant associations were observed for bacterial  
367 richness or alpha diversity with overall survival (Supplementary Figure 8). Restricting survival  
368 analyses to lung adenocarcinomas only likewise produced no significant associations  
369 (Supplementary Figure 9).

370

371 We performed power calculations to derive the minimum hazard ratios achieving 80%  
372 statistical power. Using the Bonferroni-corrected p-value thresholds (37 taxa for RNA-seq, 25  
373 taxa for 16S rRNA, and 45 taxa for WGS), the minimum hazard ratio required to achieve 80%  
374 power was approximately 1.34 for all three platforms. When using a p-value threshold of 0.01,  
375 the minimum hazard ratios to achieve 80% power were approximately 1.27 for WGS, 1.30 for  
376 RNA-seq, and 1.29 for 16S rRNA. This indicates that if there were survival associations with  
377 modest effect sizes, we would have had sufficient statistical power to detect them.

378

379 We also tested whether RNA-seq and 16S bacterial richness or diversity was associated with  
380 immune cells by leveraging paired human transcriptomic data plus cell deconvolution methods.  
381 We noted a weak positive correlation between RNA-seq genus richness and log proportion of  
382 Th1 cells in tumor tissue, and a weak negative correlation between 16S Shannon diversity and  
383 log proportion of B-cells in normal tissues. Ultimately, however, we noticed no strong,  
384 consistent trends between datasets (Supplementary Figure 10).

385

### 386 **The microbiome is not associated with human genomic features**

387

388 We took advantage of the associated human whole-genome<sup>58,59</sup> data from these same samples  
389 and investigated whether major driver mutations or fusions, copy number alterations, kataegis,  
390 or mutational signatures in the human lung cancer genome were associated with microbiome  
391 richness and alpha diversity, adjusted for study site differences (Supplementary Data 9,  
392 Supplementary Figure 11a,b). All associations between the microbiome and genomic features  
393 were not significant after multiple testing correction (Supplementary Figure 11c).

394

## 395 **DISCUSSION**

396

397 In the largest study of the LCINS microbiome to date using 16S sequencing, together with WGS  
398 and RNA-seq, we observed very low microbial abundance across over 4,000 samples, and little  
399 evidence of association between the composition or diversity of the lung cancer microbiome  
400 and LCINS tumor characteristics, genomic features, and survival.

401

402 The bulk of research on the lung microbiome to date is derived from samples collected *via*  
403 bronchoalveolar lavage (BAL), and the consensus of these studies is that the healthy lung  
404 microbiome is composed mainly of oral and tracheal commensals (e.g., genera *Streptococcus*  
405 15.7 - 38.7%, *Prevotella* 5 - 26.5%, *Veillonella* 3.8 - 4.0%, *Haemophilus* 0.02 - 15.5%, and  
406 *Neisseria* 6.5 - 9.3% among two BAL-based lung cancer studies<sup>50,52</sup>, and among the highest  
407 abundance in several other studies in cancer<sup>32,53</sup> and non-cancer<sup>28-30</sup> patients). While these  
408 genera were present in our study, they summed to a small minority of the overall microbiome

409 composition in all three data types (mean total relative abundance 4.0% - 5.8%). Instead, the  
410 highest abundance genera across all data types in tumors and normal lung were *Acinetobacter*,  
411 *Corynebacterium*, *Pseudomonas*, and *Staphylococcus*. These findings closely agree with a  
412 recent, highly decontaminated 16S sequencing dataset of 245 lung tumors (43 never smokers)<sup>35</sup>  
413 in which these genera were all among the top ten most abundant after decontamination. In  
414 blood WGS data, the most abundant bacteria were *Methylobacterium*, *Ralstonia*, *Burkholderia*,  
415 and *Pseudomonas*. Of note, abundance of phyla *Firmicutes* and *Proteobacteria* and genus  
416 *Staphylococcus* were correlated between tumor samples and paired blood. These correlations  
417 may suggest migration of these bacteria from the lung to the blood, although translocation  
418 from other organs and/or contaminations that could not be removed with the current  
419 approaches are always possible contributing factors. Nonetheless, we ultimately found no  
420 clinical associations with circulating bacteria.

421  
422 RNA-seq data showed minor differences between tumor samples and paired adjacent normal  
423 tissue in alpha or beta diversity, and an enrichment of several human commensals in normal  
424 tissue (e.g., *Corynebacterium*, *Anaerococcus*, *Finegoldia*). Tumor tissues had slightly decreased  
425 alpha diversity compared to normal tissues in both the 16S and RNA-seq datasets. However, we  
426 noted no other robust associations of microbial abundances, richness, alpha diversity, or beta  
427 diversity with any available clinical features or patient survival, no associations between the  
428 microbiome and known tumor genomic features, and no consistent trends in microbiome-  
429 immune system crosstalk.

430  
431 There are several limitations in this study. First, our normal lung tissue samples are only from  
432 lung cancer patients since lung tissue from healthy individuals can rarely be collected. Thus, we  
433 may have missed differences in the lung microbiome between healthy individuals and cancer  
434 patients. This study provides a snapshot of the microbiome at the time of tumor resection and  
435 our samples were treatment-naïve, so we could not investigate the role of microbiome on  
436 treatment response. This study lacks negative controls for RNA-seq and WGS datasets which  
437 limits identification of contaminating bacteria in these datasets. However, incomplete  
438 decontamination is more likely to result in false-positive than false-negative associations<sup>61,73</sup>.  
439 Furthermore, we leveraged state-of-the-art decontamination algorithms using negative  
440 controls in our 16S dataset and likewise produced no significant associations. Lastly, removing  
441 additional bacteria would unlikely result in positive associations given that we already have  
442 sufficient statistical power to detect associations with even modest effect sizes.

443  
444 Every null result should be interpreted with caution. As methods for bacterial sequencing and  
445 microbiome analysis evolve to better accommodate low biomass samples, it is possible that a  
446 role for the lung microbiome in cancer could be found in the future. But, as it stands, after  
447 applying multi-omics datasets with rigorous quality control and state-of-the-art analytical  
448 methods in 4,090 samples across 940 patients, the lung cancer microbiome does not appear to  
449 have a dominant role in LCINS.

450

## 451 METHODS

452

453 **Ethics declaration**

454

455 The NCI exclusively received de-identified samples and data from collaborating centers, had no  
456 direct interaction with study subjects, and did not use or generate any identifiable private  
457 information, therefore the *Sherlock-Lung* study was classified as “Not Human Subject Research  
458 (NHSR)” according to the Federal Common Rule (45 CFR 46; [eCFR.gov](http://www.ecfr.gov)). Some tissue specimens  
459 were obtained from the IUCPQ Tissue Bank, site of the Quebec Respiratory Health Network  
460 Biobank or the FQRS ([www.tissuebank.ca](http://www.tissuebank.ca)) in compliance with Institutional Review Board-  
461 approved management modalities. Some samples and data from patients included in this study  
462 were provided by the INCLIVA Biobank (PT17/0015/0049), integrated in the Spanish National  
463 Biobanks Network and in the Valencian Biobanking Network, and they were processed  
464 following standard operating procedures with the appropriate approval of the Ethics and  
465 Scientific Committees. All collaborating centers obtained informed consent for publication of  
466 human data from participants under protocols approved by their respective Institutional  
467 Review Boards (IRBs).

468

469 **Sample Collection and Handling**

470

471 Samples were collected as described in previous *Sherlock-Lung* publications<sup>57,58</sup>. We collected  
472 tumor samples from 940 patients with histologically confirmed lung cancer from various  
473 geographical regions: 220 from Taiwan; 208 from International Agency for Research on Cancer,  
474 Lyon, France, collected in Russia, Czech Republic, Romania, Serbia, and Poland; 133 from Hong  
475 Kong; 113 from Quebec City, Canada; 78 from Nice, France; 72 from Toronto, Canada; 26 from  
476 Massachusetts, USA; 22 from Connecticut, USA; 18 from Mexico City, Mexico; 13 from New  
477 York, USA; 13 from Minnesota, USA; 11 from Florida, USA; 9 from Valencia, Spain; and 4 from  
478 Lima, Peru. Fresh frozen tumor tissue and matched whole blood samples or fresh frozen normal  
479 lung tissue (collected at least 3 cm away from the tumor when possible) were obtained from  
480 these treatment-naïve patients. Genetic ancestry information was defined using WGS by  
481 clustering with the 1000 Genome Project (1KGR) reference panel with VerifyBamID2<sup>74</sup>. In the  
482 absence of WGS data, we relied on self-reported ancestry. For each patient, we reported the  
483 geographical location where the cancer was diagnosed.

484

485 We adhered to strict sample selection criteria:

- 486 1) Contamination and relatedness: Cross-sample contamination was kept below 1% using  
487 Compair<sup>75</sup>, and relatedness was maintained below 0.2 using Somalier<sup>76</sup>.
- 488 2) Copy number analysis: Subjects with abnormal copy number profiles in normal samples  
489 were excluded, as determined by Battenberg<sup>77</sup>.
- 490 3) Mutational signatures: Tumor samples exhibiting mutational signatures SBS7 (associated  
491 with ultraviolet light exposure) or SBS31 (associated with platinum chemotherapy) were  
492 excluded.
- 493 4) WGS quality control: Tumor samples with a total genomic alteration count of <100 or  
494 <1,000 and an NRPCC (number of reads per clonal copy) <10 were excluded.

495 These stringent criteria were consistently applied to ensure data robustness and reliability in  
496 the *Sherlock-Lung* study.

497

#### 498 **Whole-genome sequencing**

499

500 WGS library construction was carried out as previously reported<sup>58,59</sup>. Briefly, frozen tumor  
501 tissue along with matched blood or normal tissue samples were immediately placed into 1ml of  
502 0.2 mg/ml Proteinase K (Qiagen) in DNA lysis buffer (10 mM Tris-Cl, pH 8.0; 0.1 M EDTA, pH 8.0;  
503 0.5% SDS) and incubated for 24 hours at 56°C with shaking at 850 rpm in a Thermomixer R  
504 (Eppendorf) until completely lysed. Genomic DNA was extracted from fresh frozen tissue using  
505 the QIAamp DNA Mini Kit (Qiagen) following the manufacturer's protocol. Each sample was  
506 eluted in 200 µl AE buffer, and DNA concentration was measured using a Nanodrop  
507 spectrophotometer. All DNA samples were aliquoted and stored at -80°C until needed.

508

509 DNA was quantified using the QuantiFluor® dsDNA System (Promega Corporation, USA). DNA  
510 standardized to a concentration of 25 ng/µl and underwent fragment analysis using the  
511 AmpFLSTR™ Identifiler™ PCR Amplification Kit (ThermoFisher Scientific, USA). DNA samples  
512 were required to meet minimum mass and concentration thresholds for each assay and show  
513 no evidence of contamination or profile discordance in the Identifiler assay. Samples that met  
514 these criteria were aliquoted at the appropriate mass needed for downstream assay  
515 processing.

516

517 The Broad Institute (<https://www.broadinstitute.org>) performed WGS on the Novaseq6000  
518 platform using Illumina protocols for 2x150bp paired-end sequencing in 1246 (this study) and  
519 the Illumina HiSeq X platform ( $n=377$ ) for our previous publication<sup>58</sup>. FASTQ files were  
520 generated post-Illumina base-calling. These paired FASTQ files were converted into unmapped  
521 BAM files using the GATK pipeline (<https://github.com/gatk-workflows/seq-format-conversion>)  
522 and were then processed using GATK on the cloud-based TERRA workspaces platform  
523 (<https://app.terra.bio>). The sequencing data was then aligned to the human reference genome  
524 GATK-GRCh38, and the resulting aligned BAM files were transferred to the NIH HPC system  
525 (<https://hpc.nih.gov>) for downstream analyses.

526

#### 527 **RNA sequencing**

528

529 RNA-seq was performed using the Illumina NovaSeq6000 platform and Roche KAPA RNA  
530 HyperPrep with RiboErase protocol, generating 2x151bp paired-end reads. For human  
531 transcriptomics analyses, FASTQ files were aligned to the human reference genome GATK-  
532 GRCh38 using STAR<sup>78</sup> (v2.7.3), and were quantified using HTSeq(v2.0.4)<sup>79</sup> and GENCODE v35<sup>80</sup>.  
533 Counts data were batch corrected with ComBat-Seq<sup>81</sup>, followed by TMM normalization using  
534 DESeq2<sup>82</sup>.

535

#### 536 **16S Microbiome Sequencing**

537

538 For each sample, 100 ng of DNA, utilizing Quant-iT PicoGreen dsDNA (Thermo Fisher Scientific,  
539 Waltham, MA) quantitation, is split into 50 ng (5 ng/uL) aliquots for two separate PCR reactions.  
540 PCR was performed in 25 uL reaction volumes consisting of: 50 ng (10 uL) of DNA, 10 uL of 2X  
541 PlatinumTM Hot Start PCR Master Mix (ThermoFisher Scientific), 3 uL of MBG Water, and 2 uL  
542 of the 5  $\mu$ M 16S rRNA v4 (515f-806r) barcoded primer mix, comprised of equimolar forward and  
543 reverse primer pairs targeting the V4 region of the 16S rRNA gene<sup>83</sup>. Controls without input  
544 DNA were also included for PCR with the same reaction volumes, including a ‘water’ control  
545 with 10uL of MBG water in place of 10uL of DNA, and a ‘no template’ control with no DNA or  
546 added water. 515f forward PCR primer sequence was:

547 AATGATACGGCGACCACCGAGATCTACAC TATGGTAATT GT GTGCCAGCMGCCGCGTAA

548

549 consisting of the 5' Illumina adapter, forward primer pad, forward primer linker and forward  
550 primer. 806r reverse PCR primer sequence was:

551

552 CAAGCAGAAGACGGCATACGAGAT XXXXXXXXXXXX AGTCAGTCAG CC  
553 GGACTACHVGGGTWTCTAAT

554

555 consisting of the reverse complement of the 3' Illumina adapter, Golay barcode (12 bp barcode  
556 identifier generated specifically for this primer set to support multiplexing of samples), reverse  
557 primer pad, reverse primer linker and reverse primer (Integrated DNA Technologies, Coralville,  
558 IA). Thermal cycling was performed with the following PCR conditions: 94° C hold for 3 min,  
559 denature at 94° C for 45 s, anneal at 50° C for 1 min, extend at 72° C for 1 min 30 s for 25 cycles,  
560 followed by a 72° C hold for 10 min.

561

562 Sample PCR replicates were then pooled and purified using a 1:1 AMPure XP (Beckman Coulter  
563 Genomics, Danvers, MA) ratio, performing the final elution in 30 uL of Buffer EB (Qiagen,  
564 Germantown, MD). Amplified sample libraries were quantified using Quant-iT PicoGreen  
565 dsDNA Reagent (ThermoFisher Scientific, Waltham, MA) and up to 192, with unique barcoded  
566 adapters, were combined in equal amounts (100 ng each) and pools normalized to 10 nM with  
567 Buffer EB for pooled sequencing.

568

569 Sequencing was performed at the Cancer Genomics Research Laboratory using the Illumina  
570 MiSeq v2, 500 cycle kit (Illumina, San Diego, CA, USA) following the manufacturer's protocol<sup>84</sup>  
571 with the following modifications: Pooled libraries were diluted to 5 pM in a serial dilution, and  
572 25% denatured 5pM PhiX was spiked-in and added to the “Load Sample” well. 3.4ul of Index  
573 Sequencing Primer at 100mM, 3.4ul of Read 1 Sequencing primer at 100mM and 3.4ul of Read  
574 2 Sequencing Primer at 100uM was added to wells 13, 12 and 14 of the MiSeq sequencing  
575 cartridge. 2x251 Paired end sequencing was performed on the MiSeq, with up to 192 samples  
576 per run.

577

## 578 **Taxonomic Classification of Non-Human Reads**

579

580 For classification of RNA-seq and WGS, unaligned read pairs were extracted from GATK-  
581 GRCh38-aligned bam files. To remove additional human reads, these reads were then realigned

582 to the CHM13 T2T genome reference<sup>63</sup>, using bwa-mem<sup>85</sup> (v0.7.17) to align WGS and 16S reads,  
583 and hisat<sup>86</sup>(v2.2.2.1-ngs3.0.1) to align RNA-seq reads. Unaligned read pairs were extracted from  
584 this alignment. Reads were then trimmed using Trimmomatic<sup>87</sup> to remove trailing bases with  
585 average quality score less than 10 using a sliding window. Reads smaller than 45bp after  
586 trimming were discarded.

587

588 Taxonomic assignment of reads was performed with Kraken2<sup>64</sup> (v2.1.2) using the Kraken2  
589 standard database plus fungal and protozoan genomes downloaded on June 5th, 2023. For  
590 taxonomic assignment of RNA-seq reads the human transcriptome was also included in the  
591 database to detect unaligned human reads spanning splice junctions. WGS read counts at the  
592 genus level were adjusted using Bracken<sup>65</sup> with a minimum of 2 reads per genus required prior  
593 to readjustment, and genera with single reads were discarded. Bacterial genera with fewer than  
594 5 assigned reads in RNA-seq samples were discarded to remove false-positive assignments.  
595 Bracken was not used to adjust RNA-seq read counts as we reasoned that Bracken's genome  
596 uniqueness statistic assumes roughly even genome coverage which may be violated in cases  
597 where specific bacterial transcripts are highly upregulated.

598

599 Reads from 16S rRNA gene sequencing were taxonomically classified with Kraken2 using a  
600 Kraken2 database created from downloaded 16S gene sequences from NCBI plus human  
601 genome GRCh38.p14. This database has the advantage of using identical taxonomies with the  
602 Kraken2 standard database, which facilitates comparison between sequencing platforms. 16S  
603 sequences were assigned with Kraken2 using a confidence threshold of 0.02 due to the high  
604 degree of similarity between 16S rRNA genes at the genus level. Genus-level read counts were  
605 then adjusted using Bracken<sup>65</sup> (v2.8) with a requirement of two reads per genus prior to  
606 readjustment.

607

#### 608 *In silico sequencing and Kraken2 confidence threshold identification*

609

610 Using InSilicoSeq<sup>88</sup>(v1.0), one million HiSeq reads were simulated from GATK-GRCh38 with  
611 uniform coverage. These reads were mapped back to GATK-GRCh38 using bwa-mem<sup>85</sup>(v0.7.17),  
612 then unaligned reads were extracted and pooled with 50,000 total reads simulated in the same  
613 manner from the genomes of eleven human-associated bacteria: *Escherichia coli* (ASM584v2),  
614 *Pseudomonas aeruginosa* (ASM676v1), *Prevotella melaninogenica* (ASM14440v1), *Rothia*  
615 *mucilaginosa* (ASM17561v1), *Haemophilus parainfluenzae* (ASM19140v1), *Klebsiella*  
616 *pneumoniae* (ASM24018v2), *Staphylococcus epidermidis* (ASM609437v1), *Moraxella osloensis*  
617 (ASM155395v1), *Cutibacterium acnes* (ASM37670v1), *Streptococcus oralis* (46338\_H01), and  
618 *Corynebacterium tuberculostearicum* (ASM1672836v1). These reads were taxonomically  
619 assigned using Kraken2 with default settings, and the percentage confidence with which each  
620 read was classified was calculated. A confidence threshold of 10% was chosen as, at this level,  
621 all simulated bacterial species were identifiable and most false-positive classifications would be  
622 excluded (Supplementary Figure 12).

623

#### 624 **Decontamination**

625

626 16S sequencing samples were decontaminated on a plate-by-plate basis using the SCRUB  
627 algorithm<sup>67</sup> with default parameters and PCR well location information to track well leakage  
628 (Supplementary Figure 13).

629

630 For WGS, previous studies have used paired blood samples from whole-genome sequencing  
631 experiments to flag contaminants under the assumption that tissue-associated microbes should  
632 be statistically more prevalent in tissue compared to paired blood<sup>70</sup>. Under this hypothesis,  
633 bacteria which are equally prevalent in blood and in paired tissue would be considered  
634 contamination. However, recent research on the human blood microbiome, with special  
635 attention paid to contaminant control, has indicated that the blood contains low levels of  
636 transient bacterial DNA, including from commensals previously associated with the oral/lung  
637 microbiomes<sup>89</sup>. Further, circulating microbial DNA, likely from tumor tissue, has been suggested  
638 as a biomarker for lung cancer detection<sup>24</sup>. Finally, low bacterial read depth in the WGS samples  
639 greatly reduces the overall sensitivity of such a comparison. Thus, we chose not to use this  
640 method for decontamination in this study. Other decontamination methods, such as heuristic-  
641 based approaches<sup>89</sup> or the popular *decontam*<sup>90</sup> algorithm were considered for the WGS and  
642 RNA-seq datasets. However, assumptions made by the frequency-based method of *decontam*  
643 are not valid in low-biomass environments<sup>90</sup>.

644

645 In all datasets, bacterial genera identified as frequent NGS contaminants were removed using a  
646 list compiled by Salter et al.<sup>68</sup>, and cross-referenced with a list of human-associated bacterial  
647 pathogens<sup>69</sup>. Bacterial genera identified as frequent NGS contaminants that encompassed two  
648 or more human-associated species were rescued to avoid discarding possibly true-positive  
649 reads. All other frequent NGS contaminants were discarded (Supplementary Data 10).

650

651 Genus *Cutibacterium* was also removed after reviewing the data. *Cutibacterium* is one of the  
652 most common skin commensals and a frequent contaminator of NGS experiments<sup>68</sup>.

653 *Cutibacterium* was universally prevalent and highly abundant in our RNA-seq and WGS  
654 datasets, but infrequently observed in our 16S sequencing samples. Its removal from the WGS  
655 dataset considerably improved alpha diversity correlations and composition correlations  
656 between samples sequenced via both WGS and 16S sequencing. Furthermore, a recent lung  
657 cancer microbiome study with many negative controls showed minimal presence of  
658 *Cutibacterium* in lung tissue after decontamination<sup>35</sup>. For these reasons, *Cutibacterium* was  
659 identified as a likely contaminant and removed from the dataset. Several other skin-associated  
660 bacteria, such as *Corynebacterium* and *Staphylococcus*, did not share these properties and were  
661 therefore not removed from the dataset: they were prevalent across all datasets, they were  
662 observed in the same decontaminated lung microbiome dataset referenced above<sup>35</sup>, and they  
663 are additionally associated with the nasal microbiome<sup>91</sup> and, more generally, humid  
664 microenvironments<sup>92</sup>.

665

666 After decontamination at the genus level, reads were then adjusted at higher levels in the  
667 taxonomy as described by Dohlman et al.<sup>70</sup> Briefly, the number of reads assigned to a given  
668 bacterial OTU was multiplied by the percentage of non-contaminant reads at the next lowest  
669 taxonomic level within that OTU (e.g. family level reads are adjusted by multiplying the number

670 of reads assigned to family X by the proportion of genus-level, non-contaminant reads within  
671 family X). This process was used recursively to decontaminate from the family level to the top  
672 of the taxonomy.

673

#### 674 **Batch Correction**

675

676 WGS and RNA-seq genus- and phylum-level raw abundances (i.e. with no decontamination  
677 applied) were corrected to remove batch effects using Combat-Seq. Prior to batch correction,  
678 bacterial OTUs with prevalence less than 1% were removed in both datasets. For WGS, DNA  
679 extraction batch was used as the adjustment variable, and no biological variable was set as DNA  
680 extraction batch was partially confounded with biosample type. All RNA for this study was  
681 extracted at the same laboratory, and were therefore corrected with study site as the batch  
682 variable and tumor-normal status as the biological variable. Following batch correction,  
683 decontamination of batch-corrected counts was applied as previously described at the genus-  
684 level.

685

686 16S samples were left uncorrected as these samples did not show evidence of strong batch  
687 effects (Supplementary Figure 1f).

688

#### 689 **Differential Abundance**

690

691 Differential abundance was analyzed using the ALDEx2<sup>93</sup> and the ANCOM-BC<sup>94</sup> R packages.  
692 Bacterial taxa with prevalence less than 5% were discarded. For tumor versus normal  
693 differential abundance analysis, only subjects with paired tumor and normal lung tissue were  
694 included. For ANCOM-BC analysis, both study site and tumor-normal status were included in  
695 the differential abundance model to adjust for lingering batch effects.

696

#### 697 **Microbiome Diversity Analyses**

698

699 Microbiome diversity analyses were performed using the R package *vegan*. Genus richness was  
700 calculated as the expected number of unique bacterial genera at the specified rarefaction  
701 depths per sequencing modality. Alpha diversity analysis was performed using the Shannon  
702 index. Samples were randomly sampled to the appropriate rarefaction depth 100 times, and  
703 the median alpha diversity per sample over these 100 iterations was used downstream for  
704 alpha diversity calculations.

705

706 Beta diversity was calculated using Bray-Curtis distances with 50 random rarefaction sampling  
707 iterations at the previously specified sampling depths. Association of clinical variables with beta  
708 diversity was performed via permutational multivariate ANOVA analysis<sup>95,96</sup>, implemented in  
709 the *adonis2* function, to find the marginal variance explained by each variable over 999  
710 permutations.

711

#### 712 **Survival Analyses**

713

714 For survival analyses, Cox proportional hazards models were fit with time since diagnosis as the  
 715 time scale. Follow-up ended at death (overall survival), administrative censoring, or loss to  
 716 follow-up. All survival times were censored at ten years for survival associations. The baseline  
 717 hazards were stratified by study site, tumor stage, and age at diagnosis (age>65, age≤65).  
 718 Tumor stages II, III, and IV were combined for more robust inference. Cox proportional hazards  
 719 models were further adjusted for age at diagnosis in ten year categories.

720  
 721 For survival associations with individual bacterial abundances, only bacterial genera with at  
 722 least 50 reads in RNA-seq in at least ten percent of samples were included (this read cutoff was  
 723 relaxed to 10 in 16S and WGS to account for the lower read depth), and read counts were  
 724 transformed using center log ratio transformation<sup>97</sup> with 0.05 added as pseudo-counts to the  
 725 reads matrix.

726  
 727 **Statistical Analyses**

728  
 729 All statistical analyses were performed in R version 4.5.1. False discovery rates were calculated  
 730 using the Benjamini-Hochberg method<sup>98</sup> for multiple hypothesis testing correction. For  
 731 comparisons of continuous variables, Wilcoxon rank sums tests were employed unless  
 732 otherwise noted. Prior to correlating individual bacterial relative abundances, read counts were  
 733 transformed per-sample using center log ratio transformation with 0.05 pseudo-counts added.

734  
 735 Meta-analysis of generalized linear models and Cox models for WGS was performed using a  
 736 fixed effect model, and p-values were calculated using Fisher's combined probability test. Meta-  
 737 analysis of beta-diversity was performed by averaging  $R^2$  between the two data subsets, and p-  
 738 values were calculated using Fisher's combined probability test.

739  
 740 **Power calculations**

741  
 742 *Power for detecting difference between tumor and matched normal tissue samples*

743  
 744 For the  $\mathbb{P}^{(2)}$  subject, let  $\mathbb{P}_1^+$  be the measurement of the tumor sample and  $\mathbb{P}_1^-$  be the  
 745 measurement of the adjacent normal tissue sample. We tested the null hypothesis that the  
 746 measurement does not differ between tumor and normal tissue samples using a paired  $\mathbb{P}$ -test.  
 747 For the  $\mathbb{P}^{(2)}$  subject, define difference  $\delta_1 = \mathbb{P}_1^+ - \mathbb{P}_1^-$  and let  $\hat{\sigma}^2 = \mathbb{P}^{(2)}(\mathbb{P}_1)$ . Let effect size  $\mathbb{P} =$   
 748  $\mathbb{P}(\mathbb{P})/\mathbb{P}$ , the expected difference between tumor and normal samples normalized by standard  
 749 deviation. The noncentrality parameter (NCP) of the paired t-test  $\mathbb{P}$  is approximately  $\mathbb{P} = \mathbb{P}\sqrt{\mathbb{P}}$ ,  
 750 where  $\mathbb{P}$  is the number of subjects. Since sample size  $\mathbb{P}$  is reasonably large, we use normal  
 751 distribution to approximate the power:

752  
 753 (1)  $\mathbb{P}(|\mathbb{P}| > \mathbb{P}_1) = \mathbb{P}(\mathbb{P} > \mathbb{P}_1) + \mathbb{P}(\mathbb{P} < -\mathbb{P}_1) = \mathbb{P}(\mathbb{P} - \mathbb{P} > \mathbb{P}_1 - \mathbb{P}) + \mathbb{P}(\mathbb{P} - \mathbb{P} < -\mathbb{P}_1 - \mathbb{P})$   
 754

755 which is simplified as  $\Phi(\frac{\alpha}{\sigma}) + \Phi(-\frac{\alpha}{\sigma})$ . Here,  $\frac{\alpha}{\sigma}$  is the quantile corresponding to level  
 756  $\alpha$ , with  $\alpha$  chosen by the Bonferroni correction or  $\alpha = 0.01$ .

757

758 *Survival power analysis*

759

760 For each of the platforms (WGS, RNA-seq, 16S rRNA), we conducted power simulations by  
 761 conditioning on the observed distribution of survival times and the fraction of censoring,  
 762 assuming non-informative censoring. We assumed that survival times followed a log-normal  
 763 distribution, i.e.,  $S_i \sim \text{Exp}(\mu, \sigma^2)$ , and estimated the parameters  $\mu$  and  $\sigma^2$  by maximizing the  
 764 log-likelihood function using all available subjects with survival data. We then simulated a  
 765 microbiome feature variable  $z_i \sim \text{Exp}(0,1)$  and generated event times from the proportional  
 766 hazards model

767 (2)  $H(S_i | z_i) = H_0(S_i) \exp(\beta z_i)$

768 using the inverse probability method described by Bender et al.<sup>99</sup>. A random fraction of subjects  
 769 was selected for censoring to match the censoring rate observed in the real dataset. We applied  
 770 Cox proportional hazards regression to derive the Wald statistic for testing the null hypothesis  
 771  $H_0: \beta = 0$ . This simulation process was repeated 1,000 times, and power was calculated as the  
 772 proportion of simulations yielding a p-value below a specified threshold (either Bonferroni-  
 773 corrected or  $p = 0.01$ ).

774

775 **Identification of tumor somatic alterations**

776

777 Somatic mutation calling was conducted using our previously established bioinformatics  
 778 pipeline<sup>58</sup>. We utilized four distinct mutation calling algorithms for tumor-normal/blood paired  
 779 analysis, including Strelka<sup>100</sup> (v.2.9.10), MuTect<sup>101</sup>, MuTect2, and TNscope<sup>102</sup> within Sentieon's  
 780 genomics software(v.202010.01). An ensemble method was employed to integrate the results  
 781 from these different callers, followed by additional filtering to minimize false positives. Final  
 782 mutation calls for both single nucleotide variants (SNVs) and indels had to meet the following  
 783 criteria:

784 1) read depth >12 in tumor samples and >6 in normal samples  
 785 2) variant allele frequency <0.02 in normal samples  
 786 3) overall allele frequency (AF) <0.001 in multiple genetic databases, including 1000  
 787 Genomes (phase 3 v.5), gnomAD exomes (v.2.1.1), and gnomAD genomes (v.3.0)<sup>103</sup>

788 For indel calling, only variants identified by at least three algorithms were retained. The  
 789 IntOGen pipeline (v.2020.02.0123)<sup>104</sup>, which integrates seven advanced computational  
 790 methods, was used with default parameters to detect positive selection signals in the  
 791 mutational patterns of driver genes across the cohort.

792

793 The Battenberg algorithm<sup>77</sup> (v.2.2.9) was applied to analyze somatic copy number alterations  
794 (SCNA). Initial SCNA profiles were generated, followed by an evaluation of the clonality of each  
795 segment, purity, and ploidy. SCNA profiles deemed low-quality after manual inspection  
796 underwent a refitting process, requiring new tumor purity and ploidy inputs, either estimated  
797 by ccube<sup>105</sup> (v.1.0) or recalculated from local copy number status. The Battenberg refitting  
798 procedures were iteratively executed until the final SCNA profile met manual validation criteria.  
799 GISTIC<sup>106</sup> (v.2.0) was used to identify recurrent copy number alterations at the gene level based  
800 on the major clonal copy number for each segmentation. Structural variants (SVs) were  
801 identified using Meerkat<sup>107</sup> (v.0.189) and Manta<sup>108</sup> (v.1.6.0), applying recommended filtering,  
802 and the union of these two callers was combined to create the final SV dataset.

803

#### 804 **Tumor genomic driver mutation analysis**

805

806 To identify driver mutations among the set of recognized driver genes, we applied a  
807 comprehensive and robust strategy, incorporating several key criteria: (a) the presence of  
808 truncating mutations specifically in genes classified as tumor suppressors, (b) the recurrence of  
809 missense mutations in at least 3 samples, (c) mutations labeled as "Likely drivers" with a  
810 boostDM<sup>109</sup> score exceeding 0.5, (d) mutations classified as "Oncogenic" or "Likely Oncogenic"  
811 according to OncoKB<sup>110</sup>, (e) mutations previously identified as drivers using TCGA MC3<sup>111</sup>, and  
812 (f) missense mutations deemed "likely pathogenic" in genes annotated as tumor suppressors,  
813 as outlined by Cheng et al<sup>112</sup>. Mutations meeting any one of these criteria were considered  
814 potential driver mutations.

815

#### 816 **Mutational signature analysis**

817

818 The methods for mutational signature analysis are as previously described<sup>59</sup>. Briefly,  
819 SigProfilerMatrixGenerator<sup>113</sup> was utilized to generate mutational matrices for all types of  
820 somatic mutations, including single base substitutions (SBS), doublet base substitutions (DBS),  
821 and indels (ID). *De novo* SBS, DBS, and ID signatures were extracted using SigProfilerExtractor<sup>114</sup>  
822 (v1.1.21) with default settings, normalizing to 10,000 mutations, and using the SBS-288, DBS-78,  
823 and ID-83 mutational contexts. Subsequently, *de novo* extracted signatures were decomposed  
824 into COSMICv3.4<sup>115</sup> reference signatures based on the GRCh38 reference genome. These  
825 decomposed signatures were assigned to individual samples using SigProfilerAssignment<sup>116</sup>  
826 (v0.1.1).

827

#### 828 **RNA-seq cell-type deconvolution analysis**

829

830 For evaluation of the immune component of each sample, we used a list of immune-cell marker  
831 genes that were previously benchmarked and found to perform optimally for immune cell  
832 deconvolution in non-small cell lung cancer<sup>117,118</sup>. Samples were scored for each cell type using  
833 the median logCPM expression value among all genes within each set of cell-specific markers.

834

835 **Data Availability**

836

837 Whole genome sequencing data used in this study is deposited in the dbGaP database under  
838 accession code phs001697.v2.p1[[https://www.ncbi.nlm.nih.gov/projects/gap/cgi-  
839 bin/study.cgi?study\\_id=phs001697.v2.p1](https://www.ncbi.nlm.nih.gov/projects/gap/cgi-bin/study.cgi?study_id=phs001697.v2.p1)]. RNA-seq data used in this study is deposited in the  
840 dbGaP database under accession code phs003955.v1.p1. 16S rRNA gene sequencing data is  
841 deposited in the SRA database under BioProject accession code PRJNA1337178.

842

843 **Code Availability**

844

845 The bioinformatics pipeline can be accessed at [https://github.com/jpmcelderry/Sherlock-  
846 microbiome](https://github.com/jpmcelderry/Sherlock-microbiome).

847

848 **References**

- 849 1. on Cancer, I. A. F. R. & Others. Anonymous live flukes and *Helicobacter pylori*. *IARC Working Group  
850 on the Evaluation of Carcinogenic Risks to Humans*. Lyon France: *IARC Monogr Eval Carcinog Risks  
851 Hum* 1994; 61: 1 **241**.
- 852 2. Pleguezuelos-Manzano, C. *et al.* Mutational signature in colorectal cancer caused by genotoxic  
853 pks+ *E. coli*. *Nature* **580**, 269–273 (2020).
- 854 3. Chen, B. *et al.* Contribution of pks+ *E. coli* mutations to colorectal carcinogenesis. *Nat. Commun.*  
855 **14**, 7827 (2023).
- 856 4. Arthur, J. C. *et al.* Intestinal inflammation targets cancer-inducing activity of the microbiota.  
857 *Science* **338**, 120–123 (2012).
- 858 5. Nougayrède, J.-P. *et al.* *Escherichia coli* induces DNA double-strand breaks in eukaryotic cells.  
859 *Science* **313**, 848–851 (2006).
- 860 6. Cuevas-Ramos, G. *et al.* *Escherichia coli* induces DNA damage in vivo and triggers genomic  
861 instability in mammalian cells. *Proc. Natl. Acad. Sci. U. S. A.* **107**, 11537–11542 (2010).
- 862 7. Iftekhar, A. *et al.* Genomic aberrations after short-term exposure to colibactin-producing *E. coli*  
863 transform primary colon epithelial cells. *Nat. Commun.* **12**, 1003 (2021).
- 864 8. Cougnoux, A. *et al.* Bacterial genotoxin colibactin promotes colon tumour growth by inducing a

865 senescence-associated secretory phenotype. *Gut* **63**, 1932–1942 (2014).

866 9. Lucas, C. *et al.* Autophagy of intestinal epithelial cells inhibits colorectal carcinogenesis induced by

867 colibactin-producing *Escherichia coli* in *ApcMin/+* mice. *Gastroenterology* **158**, 1373–1388 (2020).

868 10. Lopès, A. *et al.* Colibactin-positive *Escherichia coli* induce a procarcinogenic immune environment

869 leading to immunotherapy resistance in colorectal cancer. *Int. J. Cancer* **146**, 3147–3159 (2020).

870 11. Wu, S. *et al.* A human colonic commensal promotes colon tumorigenesis via activation of T helper

871 type 17 T cell responses. *Nat. Med.* **15**, 1016–1022 (2009).

872 12. Chung, L. *et al.* *Bacteroides fragilis* toxin coordinates a pro-carcinogenic inflammatory cascade via

873 targeting of colonic epithelial cells. *Cell Host Microbe* **23**, 421 (2018).

874 13. Geis, A. L. *et al.* Regulatory T-cell response to enterotoxigenic *Bacteroides fragilis* colonization

875 triggers IL17-dependent colon carcinogenesis. *Cancer Discov.* **5**, 1098–1109 (2015).

876 14. Hwang, S. *et al.* Enterotoxigenic *Bacteroides fragilis* infection exacerbates tumorigenesis in

877 AOM/DSS mouse model. *Int. J. Med. Sci.* **17**, 145–152 (2020).

878 15. Thiele Orberg, E. *et al.* The myeloid immune signature of enterotoxigenic *Bacteroides fragilis*-

879 induced murine colon tumorigenesis. *Mucosal Immunol.* **10**, 421–433 (2017).

880 16. Wu, S., Morin, P. J., Maouyo, D. & Sears, C. L. *Bacteroides fragilis* enterotoxin induces c-Myc

881 expression and cellular proliferation. *Gastroenterology* **124**, 392–400 (2003).

882 17. Rubinstein, M. R. *et al.* *Fusobacterium nucleatum* promotes colorectal carcinogenesis by

883 modulating E-cadherin/β-catenin signaling via its FadA adhesin. *Cell Host Microbe* **14**, 195–206

884 (2013).

885 18. Rubinstein, M. R. *et al.* *Fusobacterium nucleatum* promotes colorectal cancer by inducing Wnt/β-

886 catenin modulator Annexin A1. *EMBO Rep.* **20**, e47638 (2019).

887 19. Guo, P. *et al.* FadA promotes DNA damage and progression of *Fusobacterium nucleatum*-induced

888 colorectal cancer through up-regulation of chk2. *J. Exp. Clin. Cancer Res.* **39**, 202 (2020).

889 20. Abed, J. *et al.* Fap2 mediates *Fusobacterium nucleatum* colorectal adenocarcinoma enrichment by  
890 binding to tumor-expressed Gal-GalNAc. *Cell Host Microbe* **20**, 215–225 (2016).

891 21. Casasanta, M. A. *et al.* *Fusobacterium nucleatum* host-cell binding and invasion induces IL-8 and  
892 CXCL1 secretion that drives colorectal cancer cell migration. *Sci. Signal.* **13**, eaba9157 (2020).

893 22. Gur, C. *et al.* Binding of the Fap2 protein of *Fusobacterium nucleatum* to human inhibitory receptor  
894 TIGIT protects tumors from immune cell attack. *Immunity* **42**, 344–355 (2015).

895 23. Sepich-Poore, G. D. *et al.* Robustness of cancer microbiome signals over a broad range of  
896 methodological variation. *Oncogene* **43**, 1127–1148 (2024).

897 24. Chen, H. *et al.* Circulating microbiome DNA as biomarkers for early diagnosis and recurrence of  
898 lung cancer. *Cell Rep. Med.* 101499 (2024).

899 25. Zaidi, A. H. *et al.* A blood-based circulating microbial metagenomic panel for early diagnosis and  
900 prognosis of oesophageal adenocarcinoma. *Br. J. Cancer* **127**, 2016–2024 (2022).

901 26. Park, E. M. *et al.* Targeting the gut and tumor microbiota in cancer. *Nat. Med.* **28**, 690–703 (2022).

902 27. Dickson, R. P., Erb-Downward, J. R., Martinez, F. J. & Huffnagle, G. B. The microbiome and the  
903 respiratory tract. *Annu. Rev. Physiol.* **78**, 481–504 (2016).

904 28. Hilty, M. *et al.* Disordered microbial communities in asthmatic airways. *PLoS One* **5**, e8578 (2010).

905 29. Dickson, R. P. *et al.* Bacterial topography of the healthy human lower respiratory tract. *MBio* **8**,  
906 (2017).

907 30. Charlson, E. S. *et al.* Topographical continuity of bacterial populations in the healthy human  
908 respiratory tract. *Am. J. Respir. Crit. Care Med.* **184**, 957–963 (2011).

909 31. Hasegawa, A. *et al.* Detection and identification of oral anaerobes in intraoperative bronchial fluids  
910 of patients with pulmonary carcinoma. *Microbiol. Immunol.* **58**, 375–381 (2014).

911 32. Kim, G. *et al.* Prediction of lung cancer using novel biomarkers based on microbiome profiling of  
912 bronchoalveolar lavage fluid. *Sci. Rep.* **14**, 1691 (2024).

913 33. Carney, S. M. *et al.* Methods in lung microbiome research. *Am. J. Respir. Cell Mol. Biol.* **62**, 283–299

914 (2020).

915 34. Yu, G. *et al.* Characterizing human lung tissue microbiota and its relationship to epidemiological

916 and clinical features. *Genome Biol.* **17**, 163 (2016).

917 35. Nejman, D. *et al.* The human tumor microbiome is composed of tumor type-specific intracellular

918 bacteria. *Science* **368**, 973–980 (2020).

919 36. Peters, B. A. *et al.* The microbiome in lung cancer tissue and recurrence-free survival. *Cancer*

920 *Epidemiol. Biomarkers Prev.* **28**, 731–740 (2019).

921 37. Greathouse, K. L. *et al.* Interaction between the microbiome and TP53 in human lung cancer.

922 *Genome Biol.* **19**, 123 (2018).

923 38. Apopa, P. L. *et al.* PARP1 is up-regulated in non-small cell lung cancer tissues in the presence of the

924 cyanobacterial toxin microcystin. *Front. Microbiol.* **9**, 1757 (2018).

925 39. Zheng, L. *et al.* Intact lung tissue and bronchoalveolar lavage fluid are both suitable for the

926 evaluation of murine lung microbiome in acute lung injury. *Microbiome* **12**, (2024).

927 40. Natalini, J. G., Singh, S. & Segal, L. N. The dynamic lung microbiome in health and disease. *Nat. Rev.*

928 *Microbiol.* **21**, 222–235 (2022).

929 41. Soler, N. *et al.* Airway inflammation and bronchial microbial patterns in patients with stable chronic

930 obstructive pulmonary disease. *Eur. Respir. J.* **14**, 1015–1022 (1999).

931 42. Bresser, P., Out, T. A., van Alphen, L., Jansen, H. M. & Lutter, R. Airway inflammation in

932 nonobstructive and obstructive chronic bronchitis with chronic haemophilus influenzae airway

933 infection. Comparison with noninfected patients with chronic obstructive pulmonary disease. *Am.*

934 *J. Respir. Crit. Care Med.* **162**, 947–952 (2000).

935 43. Sethi, S., Maloney, J., Grove, L., Wrona, C. & Berenson, C. S. Airway inflammation and bronchial

936 bacterial colonization in chronic obstructive pulmonary disease. *Am. J. Respir. Crit. Care Med.* **173**,

937 991–998 (2006).

938 44. Parameswaran, G. I., Wrona, C. T., Murphy, T. F. & Sethi, S. *Moraxella catarrhalis* acquisition,  
939 airway inflammation and protease-antiprotease balance in chronic obstructive pulmonary disease.

940 *BMC Infect. Dis.* **9**, 178 (2009).

941 45. Teo, S. M. *et al.* The infant nasopharyngeal microbiome impacts severity of lower respiratory  
942 infection and risk of asthma development. *Cell Host Microbe* **17**, 704–715 (2015).

943 46. Teo, S. M. *et al.* Airway Microbiota dynamics uncover a critical window for interplay of pathogenic  
944 bacteria and allergy in childhood respiratory disease. *Cell Host Microbe* **24**, 341-352.e5 (2018).

945 47. Bosch, A. A. T. M. *et al.* Maturation of the infant respiratory Microbiota, environmental drivers, and  
946 health consequences. A prospective cohort study. *Am. J. Respir. Crit. Care Med.* **196**, 1582–1590  
947 (2017).

948 48. O'Dwyer, D. N. *et al.* Lung Microbiota contribute to pulmonary inflammation and disease  
949 progression in pulmonary fibrosis. *Am. J. Respir. Crit. Care Med.* **199**, 1127–1138 (2019).

950 49. Hosang, L. *et al.* The lung microbiome regulates brain autoimmunity. *Nature* **603**, 138–144 (2022).

951 50. Lee, S. H. *et al.* Characterization of microbiome in bronchoalveolar lavage fluid of patients with  
952 lung cancer comparing with benign mass like lesions. *Lung Cancer* **102**, 89–95 (2016).

953 51. Cameron, S. J. S. *et al.* A pilot study using metagenomic sequencing of the sputum microbiome  
954 suggests potential bacterial biomarkers for lung cancer. *PLoS One* **12**, e0177062 (2017).

955 52. Hosgood, H. D., III *et al.* The potential role of lung microbiota in lung cancer attributed to  
956 household coal burning exposures. *Environ. Mol. Mutagen.* **55**, 643–651 (2014).

957 53. Liu, H.-X. *et al.* Difference of lower airway microbiome in bilateral protected specimen brush  
958 between lung cancer patients with unilateral lobar masses and control subjects. *Int. J. Cancer* **142**,  
959 769–778 (2018).

960 54. Tsay, J.-C. J. *et al.* Airway Microbiota is associated with upregulation of the PI3K pathway in lung

961 cancer. *Am. J. Respir. Crit. Care Med.* **198**, 1188–1198 (2018).

962 55. Gomes, S. *et al.* Profiling of lung microbiota discloses differences in adenocarcinoma and squamous

963 cell carcinoma. *Sci. Rep.* **9**, 12838 (2019).

964 56. Tsay, J.-C. J. *et al.* Lower airway dysbiosis affects lung cancer progression. *Cancer Discov.* **11**, 293–

965 307 (2021).

966 57. Landi, M. T. *et al.* Tracing Lung Cancer Risk Factors Through Mutational Signatures in Never-

967 Smokers : The Sherlock-Lung Study. *Am. J. Epidemiol.* **190**, 962–976 (2020).

968 58. Zhang, T. *et al.* Genomic and evolutionary classification of lung cancer in never smokers. *Nat.*

969 *Genet.* **53**, 1348–1359 (2021).

970 59. Díaz-Gay, M. *et al.* The mutagenic forces shaping the genomic landscape of lung cancer in never

971 smokers. *medRxiv* (2024) doi:10.1101/2024.05.15.24307318.

972 60. Poore, G. D. *et al.* Microbiome analyses of blood and tissues suggest cancer diagnostic approach.

973 *Nature* **579**, 567–574 (2020).

974 61. Gihawi, A. *et al.* Major data analysis errors invalidate cancer microbiome findings. *MBio* **14**,

975 e0160723 (2023).

976 62. Poore, G. D. *et al.* Retraction Note: Microbiome analyses of blood and tissues suggest cancer

977 diagnostic approach. *Nature* (2024) doi:10.1038/s41586-024-07656-x.

978 63. Rhee, A. *et al.* The complete sequence of a human Y chromosome. *Nature* **621**, 344–354 (2023).

979 64. Wood, D. E., Lu, J. & Langmead, B. Improved metagenomic analysis with Kraken 2. *Genome Biol.*

980 **20**, 257 (2019).

981 65. Lu, J., Breitwieser, F. P., Thielen, P. & Salzberg, S. L. Bracken: estimating species abundance in

982 metagenomics data. *PeerJ Comput. Sci.* **3**, e104 (2017).

983 66. Walker, S. P. *et al.* Non-specific amplification of human DNA is a major challenge for 16S rRNA gene

984 sequence analysis. *Sci. Rep.* **10**, 16356 (2020).

985 67. Austin, G. I. *et al.* Contamination source modeling with SCRuB improves cancer phenotype  
986 prediction from microbiome data. *Nat. Biotechnol.* (2023) doi:10.1038/s41587-023-01696-w.

987 68. Salter, S. J. *et al.* Reagent and laboratory contamination can critically impact sequence-based  
988 microbiome analyses. *BMC Biol.* **12**, 87 (2014).

989 69. Shaw, L. P. *et al.* The phylogenetic range of bacterial and viral pathogens of vertebrates. *Mol. Ecol.*  
990 **29**, 3361–3379 (2020).

991 70. Dohlman, A. B. *et al.* The cancer microbiome atlas: a pan-cancer comparative analysis to  
992 distinguish tissue-resident microbiota from contaminants. *Cell Host Microbe* **29**, 281-298.e5 (2021).

993 71. Pan-cancer analysis of whole genomes. *Nature* **578**, 82–93 (2020).

994 72. Robinson, K. M., Crabtree, J., Mattick, J. S. A., Anderson, K. E. & Dunning Hotopp, J. C.  
995 Distinguishing potential bacteria-tumor associations from contamination in a secondary data  
996 analysis of public cancer genome sequence data. *Microbiome* **5**, 9 (2017).

997 73. Kennedy, K. M. *et al.* Questioning the fetal microbiome illustrates pitfalls of low-biomass microbial  
998 studies. *Nature* **613**, 639–649 (2023).

999 74. Zhang, F. *et al.* Ancestry-agnostic estimation of DNA sample contamination from sequence reads.  
1000 *Genome Res.* **30**, 185–194 (2020).

1001 75. Bergmann, E. A., Chen, B.-J., Arora, K., Vacic, V. & Zody, M. C. Conpair: concordance and  
1002 contamination estimator for matched tumor-normal pairs. *Bioinformatics* **32**, 3196–3198 (2016).

1003 76. Pedersen, B. S. *et al.* Somalier: rapid relatedness estimation for cancer and germline studies using  
1004 efficient genome sketches. *Genome Med.* **12**, 62 (2020).

1005 77. Nik-Zainal, S. *et al.* The life history of 21 breast cancers. *Cell* **149**, 994–1007 (2012).

1006 78. Dobin, A. *et al.* STAR: ultrafast universal RNA-seq aligner. *Bioinformatics* **29**, 15–21 (2013).

1007 79. Anders, S., Pyl, P. T. & Huber, W. HTSeq--a Python framework to work with high-throughput  
1008 sequencing data. *Bioinformatics* **31**, 166–169 (2015).

1009 80. Frankish, A. *et al.* GENCODE reference annotation for the human and mouse genomes. *Nucleic*  
1010 *Acids Res.* **47**, D766–D773 (2019).

1011 81. Zhang, Y., Parmigiani, G. & Johnson, W. E. ComBat-seq: batch effect adjustment for RNA-seq count  
1012 data. *NAR Genom. Bioinform.* **2**, lqaa078 (2020).

1013 82. Love, M. I., Huber, W. & Anders, S. Moderated estimation of fold change and dispersion for RNA-  
1014 seq data with DESeq2. *Genome Biol.* **15**, 550 (2014).

1015 83. Caporaso, J. G. *et al.* Global patterns of 16S rRNA diversity at a depth of millions of sequences per  
1016 sample. *Proc. Natl. Acad. Sci. U. S. A.* **108 Suppl 1**, 4516–4522 (2011).

1017 84. Caporaso, J. G. *et al.* Ultra-high-throughput microbial community analysis on the Illumina HiSeq  
1018 and MiSeq platforms. *ISME J.* **6**, 1621–1624 (2012).

1019 85. Li, H. Aligning sequence reads, clone sequences and assembly contigs with BWA-MEM. *arXiv [q-  
1020 bio.GN]* (2013).

1021 86. Zhang, Y., Park, C., Bennett, C., Thornton, M. & Kim, D. Rapid and accurate alignment of nucleotide  
1022 conversion sequencing reads with HISAT-3N. *Genome Res.* **31**, 1290–1295 (2021).

1023 87. Bolger, A. M., Lohse, M. & Usadel, B. Trimmomatic: a flexible trimmer for Illumina sequence data.  
1024 *Bioinformatics* **30**, 2114–2120 (2014).

1025 88. Gourlé, H., Karlsson-Lindsjö, O., Hayer, J. & Bongcam-Rudloff, E. Simulating Illumina metagenomic  
1026 data with InSilicoSeq. *Bioinformatics* **35**, 521–522 (2019).

1027 89. Tan, C. C. S. *et al.* No evidence for a common blood microbiome based on a population study of  
1028 9,770 healthy humans. *Nat. Microbiol.* **8**, 973–985 (2023).

1029 90. Davis, N. M., Proctor, D. M., Holmes, S. P., Relman, D. A. & Callahan, B. J. Simple statistical  
1030 identification and removal of contaminant sequences in marker-gene and metagenomics data.  
1031 *Microbiome* **6**, 226 (2018).

1032 91. Human Microbiome Project Consortium. Structure, function and diversity of the healthy human

1033 microbiome. *Nature* **486**, 207–214 (2012).

1034 92. Byrd, A. L., Belkaid, Y. & Segre, J. A. The human skin microbiome. *Nat. Rev. Microbiol.* **16**, 143–155  
1035 (2018).

1036 93. Fernandes, A. D., Macklaim, J. M., Linn, T. G., Reid, G. & Gloor, G. B. ANOVA-like differential  
1037 expression (ALDEx) analysis for mixed population RNA-Seq. *PLoS One* **8**, e67019 (2013).

1038 94. Lin, H. & Peddada, S. D. Analysis of compositions of microbiomes with bias correction. *Nat.*  
1039 *Commun.* **11**, 3514 (2020).

1040 95. McArdle, B. H. & Anderson, M. J. Fitting multivariate models to community data: A comment on  
1041 distance-based redundancy analysis. *Ecology* **82**, 290–297 (2001).

1042 96. Anderson, M. J. A new method for non-parametric multivariate analysis of variance. *Austral Ecol.*  
1043 **26**, 32–46 (2001).

1044 97. Aitchison, J. The statistical analysis of compositional data. *J. R. Stat. Soc. Series B Stat. Methodol.*  
1045 **44**, 139–160 (1982).

1046 98. Benjamini, Y. & Hochberg, Y. Controlling the false discovery rate: A practical and powerful  
1047 approach to multiple testing. *J. R. Stat. Soc. Series B Stat. Methodol.* **57**, 289–300 (1995).

1048 99. Bender, R., Augustin, T. & Blettner, M. Generating survival times to simulate Cox proportional  
1049 hazards models. *Stat. Med.* **24**, 1713–1723 (2005).

1050 100. Kim, S. *et al.* Strelka2: fast and accurate calling of germline and somatic variants. *Nat. Methods* **15**,  
1051 591–594 (2018).

1052 101. Cibulskis, K. *et al.* Sensitive detection of somatic point mutations in impure and heterogeneous  
1053 cancer samples. *Nat. Biotechnol.* **31**, 213–219 (2013).

1054 102. Freed, D., Pan, R. & Aldana, R. TNscope: Accurate Detection of Somatic Mutations with Haplotype-  
1055 based Variant Candidate Detection and Machine Learning Filtering. *bioRxiv* 250647 (2018)

1056 doi:10.1101/250647.

1057 103. Karczewski, K. J. *et al.* The mutational constraint spectrum quantified from variation in 141,456

1058 humans. *Nature* **581**, 434–443 (2020).

1059 104. Martínez-Jiménez, F. *et al.* A compendium of mutational cancer driver genes. *Nat. Rev. Cancer* **20**,

1060 555–572 (2020).

1061 105. Yuan, K., Macintyre, G., Liu, W., PCAWG-11 working group & Markowetz, F. Ccube: A fast and

1062 robust method for estimating cancer cell fractions. *bioRxiv* 484402 (2018) doi:10.1101/484402.

1063 106. Mermel, C. H. *et al.* GISTIC2.0 facilitates sensitive and confident localization of the targets of focal

1064 somatic copy-number alteration in human cancers. *Genome Biol.* **12**, R41 (2011).

1065 107. Yang, L. *et al.* Diverse mechanisms of somatic structural variations in human cancer genomes. *Cell*

1066 **153**, 919–929 (2013).

1067 108. Chen, X. *et al.* Manta: rapid detection of structural variants and indels for germline and cancer

1068 sequencing applications. *Bioinformatics* **32**, 1220–1222 (2016).

1069 109. Muiños, F., Martínez-Jiménez, F., Pich, O., Gonzalez-Perez, A. & Lopez-Bigas, N. In silico saturation

1070 mutagenesis of cancer genes. *Nature* **596**, 428–432 (2021).

1071 110. Chakravarty, D. *et al.* OncoKB: A Precision Oncology Knowledge Base. *JCO Precis Oncol* **2017**,

1072 (2017).

1073 111. Bailey, M. H. *et al.* Comprehensive Characterization of Cancer Driver Genes and Mutations. *Cell*

1074 **174**, 1034–1035 (2018).

1075 112. Cheng, J. *et al.* Accurate proteome-wide missense variant effect prediction with AlphaMissense.

1076 *Science* **381**, eadg7492 (2023).

1077 113. Bergstrom, E. N. *et al.* SigProfilerMatrixGenerator: a tool for visualizing and exploring patterns of

1078 small mutational events. *BMC Genomics* **20**, 685 (2019).

1079 114. Islam, S. M. A. *et al.* Uncovering novel mutational signatures by de novo extraction with

1080 SigProfilerExtractor. *Cell Genom* **2**, None (2022).

1081 115. Sondka, Z. *et al.* COSMIC: a curated database of somatic variants and clinical data for cancer.

1082 *Nucleic Acids Res.* **52**, D1210–D1217 (2024).

1083 116. Díaz-Gay, M. *et al.* Assigning mutational signatures to individual samples and individual somatic

1084 mutations with SigProfilerAssignment. *Bioinformatics* **39**, (2023).

1085 117. Danaher, P. *et al.* Gene expression markers of Tumor Infiltrating Leukocytes. *J. Immunother. Cancer*

1086 **5**, (2017).

1087 118. Rosenthal, R. *et al.* Neoantigen-directed immune escape in lung cancer evolution. *Nature* **567**,

1088 479–485 (2019).

1089 **Acknowledgements**

1090

1091 This work was supported by the Intramural Research Program of the National Cancer Institute,  
1092 US National Institutes of Health (NIH) (project ZIACP101231 to MTL). The contributions of the  
1093 NIH authors were made as part of their official duties as NIH federal employees, are in  
1094 compliance with agency policy requirements, and are considered Works of the United States  
1095 Government. However, the findings and conclusions presented in this paper are those of the  
1096 authors and do not necessarily reflect the views of the NIH or the U.S. Department of Health  
1097 and Human Services. Additional funds were NIH grants R01ES032547-01, R01CA269919-01, and  
1098 1U01CA290479-01 to LBA as well as by LBA's Packard Fellowship for Science and Engineering,  
1099 and by NIH grant U01CA209414 to DCC to support the Boston Lung Cohort Study. Where  
1100 authors are identified as personnel of the International Agency for Research on Cancer/World  
1101 Health Organization, the authors alone are responsible for the views expressed in this article  
1102 and they do not necessarily represent the decisions, policy or views of the International Agency  
1103 for Research on Cancer/World Health Organization. We want to particularly acknowledge the  
1104 patients and the INCLIVA Biobank (PT17/0015/0049) integrated in the Spanish National  
1105 Biobanks Network and in the Valencian Biobanking Network for their collaboration. This study  
1106 was supported by the Health and Medical Research Fund of Hong Kong SAR, HMRF 03142856.  
1107 The related studies of Taiwan site were supported by grants from the Ministry of Health and  
1108 Welfare, Taiwan DOH97-TD-G-111-026 (C.A.H.), DOH98-TD-G-111-015 (C.A.H.), DOH99-TD-G-  
1109 111-028 (C.A.H.); DOH97-TD-G-111-029 (C.Y.C.), DOH98-TD-G-111-018 (C.Y.C.), DOH99-TD-G-  
1110 111-015 (C.Y.C.) and the Ministry of Science and Technology, Taiwan MOST109-2740-B-400-002  
1111 (C.A.H.), MOST110-2740-B-400-002 (C.A.H.), MOST111-2740-B-400-002 (C.A.H.). This work has  
1112 been supported in part by the Tissue Core at the H. Lee Moffitt Cancer Center & Research  
1113 Institute, a comprehensive cancer center designated by the National Cancer Institute and  
1114 funded in part by a Moffitt Cancer Center Support Grant (no. P30-CA076292). The authors  
1115 would like to thank the team at the IUCPQ site of the Quebec Respiratory Health Network  
1116 Biobank of the FRQS for their valuable assistance, and would like to thank the staff at Harvard  
1117 University, Yale University, Roswell Park Cancer Institute and Roswell PI, Instituto Nacional de

1118 Cancerologia, Nice University Hospital Centre (Nice UHC) - University Côte d'Azur and the Nice  
1119 Biobank CRB, Toronto University Health Network, and Mayo Clinic for their assistance providing  
1120 samples and corresponding clinical data. The computational analyses reported in this  
1121 manuscript have utilized the NIH high-performance Biowulf Cluster. We thank the study  
1122 participants and the staff at Westat Inc. for their assistance in collecting samples and  
1123 corresponding clinical data. We would like to thank Ruth Pfeiffer for her advice on survival  
1124 analyses.

1125

#### 1126 **Author Contributions**

1127

1128 Conceptualization: MTL, JPM;  
1129 Methodology: JPM, JSh, TZ, JS, AK, MS, OL, SS, KMJ, MAN, MTL;  
1130 Formal Analysis: JPM, TZ, WZ, EV, CCA, BZ, MD-G, DCW, LBA, JSh, SA-S;  
1131 Pathology work: RH; S-RY; LMS; CL; MKB; PJ; WDT;  
1132 Management: PHoa;  
1133 Resources: LM, OGAR, ESE, JMS, MBS, SSY, MMA, JL, BS, AM, OS, DZ, IH, VJ, DM, SM, MS, MK,  
1134 YB, BEGR, DCC, VG, PB, GL, PHof, MPW, KCL, C-YC, CAH, NR, QL, MTL, SJC;  
1135 Data Curation: PHoa, TZ, WZ, CH, FJC-M, MMi;  
1136 Writing, Original Draft: JPM, JSh, MTL;  
1137 Writing, Review & Editing: All authors;  
1138 Visualization: JPM, TZ, MTL;  
1139 Supervision: MTL.

1140

#### 1141 **Competing Interests**

1142

1143 LBA is a co-founder, CSO, scientific advisory member, and consultant for io9, has equity and  
1144 receives income. The terms of this arrangement have been reviewed and approved by the  
1145 University of California, San Diego in accordance with its conflict of interest policies. LBA is also  
1146 a compensated member of the scientific advisory board of Inocras. LBA's spouse is an employee  
1147 of Biotheranostics. ENB and LBA declare U.S. provisional patent application filed with UCSD  
1148 with serial numbers 63/269,033. LBA also declares U.S. provisional applications filed with UCSD  
1149 with serial numbers: 63/366,392; 63/289,601; 63/483,237; 63/412,835; and 63/492,348. LBA is  
1150 also an inventor of a US Patent 10,776,718 for source identification by non-negative matrix  
1151 factorization. SRY has received consulting fees from AstraZeneca, Sanofi, Amgen, AbbVie, and  
1152 Sanofi; received speaking fees from AstraZeneca, Medscape, PRIME Education, and Medical  
1153 Learning Institute. All other authors declare that they have no competing interests.

1154

1155 **Table 1.** Demographic and clinical features of study subjects

Characteristic	16S N = 701 <sup>1</sup>	RNA N = 661 <sup>1</sup>	WGS N = 811 <sup>1</sup>
<b>Age At Diagnosis</b>			
Unknown	64 (57, 72)	64 (57, 72)	65 (58, 72)
Female	0	0	4
<b>Sex</b>			
Male	563 (80%)	529 (80%)	639 (79%)
Female	138 (20%)	132 (20%)	172 (21%)
<b>Ancestry</b>			
African (AFR)	2 (0.3%)	0 (0%)	4 (0.5%)
American (AMR) or Mixed	38 (5.4%)	39 (5.9%)	28 (3.5%)
East Asian (EAS)	388 (55%)	354 (54%)	338 (42%)
European (EUR)	272 (39%)	267 (40%)	441 (54%)
Unknown	1	1	0
<b>Study Site</b>			
Connecticut, USA	0 (0%)	0 (0%)	22 (2.7%)
Florida, USA	0 (0%)	0 (0%)	11 (1.4%)
Hong Kong	132 (19%)	130 (20%)	113 (14%)
IARC (Serbia, Czech Republic, Romania, Poland, Russia)	204 (29%)	195 (30%)	190 (23%)
Lima, Peru	4 (0.6%)	4 (0.6%)	0 (0%)
Massachusetts, USA	0 (0%)	0 (0%)	26 (3.2%)
Mexico City, Mexico	14 (2.0%)	16 (2.4%)	0 (0%)
Minnesota, USA	12 (1.7%)	13 (2.0%)	13 (1.6%)
New York, USA	12 (1.7%)	11 (1.7%)	13 (1.6%)
Nice, France	26 (3.7%)	44 (6.7%)	53 (6.5%)
Quebec, Canada	0 (0%)	0 (0%)	113 (14%)
Taiwan	218 (31%)	202 (31%)	184 (23%)
Toronto, Canada	71 (10%)	39 (5.9%)	68 (8.4%)
Valencia, Spain	8 (1.1%)	7 (1.1%)	5 (0.6%)
<b>Stage</b>			
I	407 (61%)	368 (59%)	496 (64%)
II	115 (17%)	113 (18%)	131 (17%)
III	108 (16%)	107 (17%)	120 (15%)
IV	38 (5.7%)	39 (6.2%)	30 (3.9%)
Unknown	33	34	34
<b>Histology Composite</b>			
Adenocarcinoma	621 (89%)	584 (88%)	695 (86%)
Adenosquamous carcinoma	12 (1.7%)	9 (1.4%)	11 (1.4%)
Carcinoid tumor	23 (3.3%)	23 (3.5%)	58 (7.2%)
Squamous cell carcinoma	36 (5.1%)	36 (5.4%)	34 (4.2%)
Other	9 (1.3%)	9 (1.4%)	13 (1.6%)

<sup>1</sup>Median (Q1, Q3); n (%)

1157 **Table 2:** Read Depth statistics per sequencing modality and sample type.  
1158

Tumor-Normal Status	n	mean	median	Standard Deviation	Range	
					Low	High
<b>16S</b>						
Tumor	701	66,917	61,644	31,947	4,024	199,104
Normal	563	57,628	58,308	20,127	5,166	194,827
<b>RNAseq</b>						
Tumor	661	129,635,580	127,478,501	38,900,833	22,429,409	610,965,375
Normal	542	130,148,355	126,346,728	37,999,097	20,866,863	471,422,274
<b>WGS</b>						
Blood	447	942,996,840	908,564,834	189,070,286	680,579,372	1,814,647,436
Tumor	811	2,348,912,898	2,292,893,294	330,902,893	727,878,974	4,382,840,738
Normal	365	941,838,237	925,300,124	166,991,678	659,749,314	2,299,531,502

1159

1160

1161 **Main Figure Legends**

1162 **Figure 1:** General overview of the pipeline and dataset. a) Count of samples per combinations  
1163 of sequencing platforms, by biospecimen type. b) Overview of the analytical pipeline used for  
1164 this study. Bracken abundance estimation was used only with WGS (combining this study and  
1165 Zhang et al. 2021) and 16S. After decontamination, read counts above the genus level were  
1166 recursively adjusted (Methods). Created in BioRender. McElderry, J. (2025) <https://BioRender.com/8kkrqgu>. c) Total reads assigned to different domains and to the human  
1167 genome (WGS  $n= 1176$ ; RNA-seq  $n=1203$ , 16S  $n=1264$ ). d)  $\log_{10}$  bacterial reads per million,  
1168 including human and other sequences, by sequencing modality and tissue type (WGS  $n= 811$   
1169 tumors, 365 normal lung, 447 blood samples; RNA-seq  $n= 661$  tumors, 542 normal lung  
1170 samples; 16S  $n=701$  tumors, 563 normal lung samples). e)  $\log_{10}$  absolute bacterial read counts  
1171 by sequencing modality and tissue type (WGS  $n= 811$  tumors, 365 normal lung, 447 blood  
1172 samples; RNA-seq  $n= 661$  tumors, 542 normal lung samples; 16S  $n=701$  tumors, 563 normal  
1173 lung samples). f) Comparison of  $\log_{10}$  per-million genus-level bacterial reads in the WGS dataset  
1174 compared to WGS from other studies. Boxplot centers, upper and lower bounds, and whiskers  
1175 represent median, upper and lower quartiles, and quartiles  $\pm 1.5$  inter-quartile range,  
1176 respectively. WGS = whole genome sequencing; Rna-seq = RNA sequencing; 16S = 16S rRNA  
1177 gene sequencing.

1179

1180 **Figure 2:** Compositional overview of each dataset after decontamination. a) Overview of the  
1181 phylum-level relative abundances for all samples in this dataset, ordered by abundance of  
1182 Proteobacteria. b) Mean phylum-level and c) genus-level relative abundances by sequencing  
1183 platform and tumor-normal status, including only samples which were sequenced across all  
1184 three sequencing modalities. d) Rarefaction curve showing the relationship between read  
1185 depth and number of unique bacterial genera observed in 16S, RNA-seq, and WGS datasets  
1186 across all tissue types. WGS = whole genome sequencing; RNA-seq = RNA sequencing; 16S = 16S  
1187 rRNA gene sequencing.

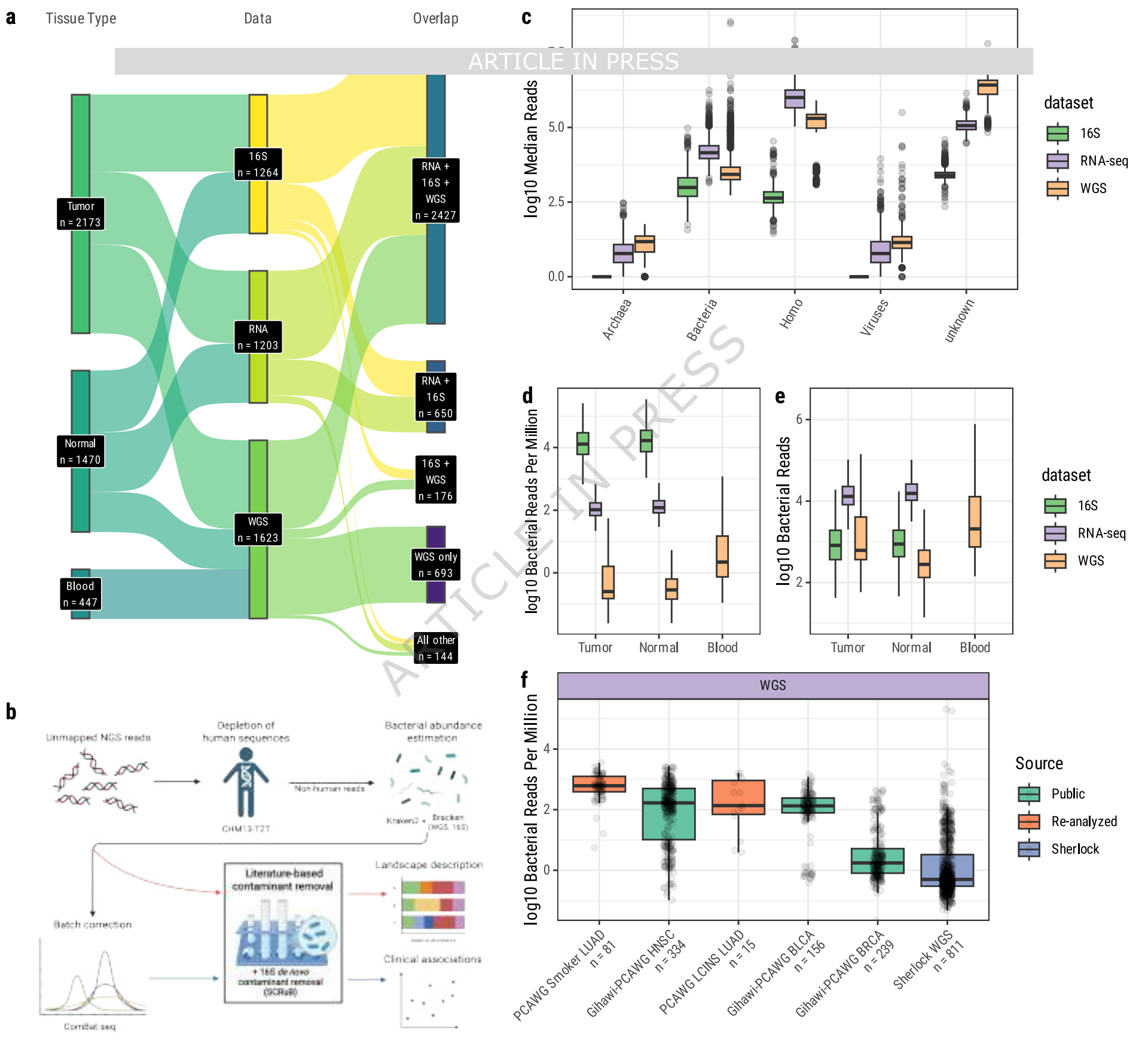
1188

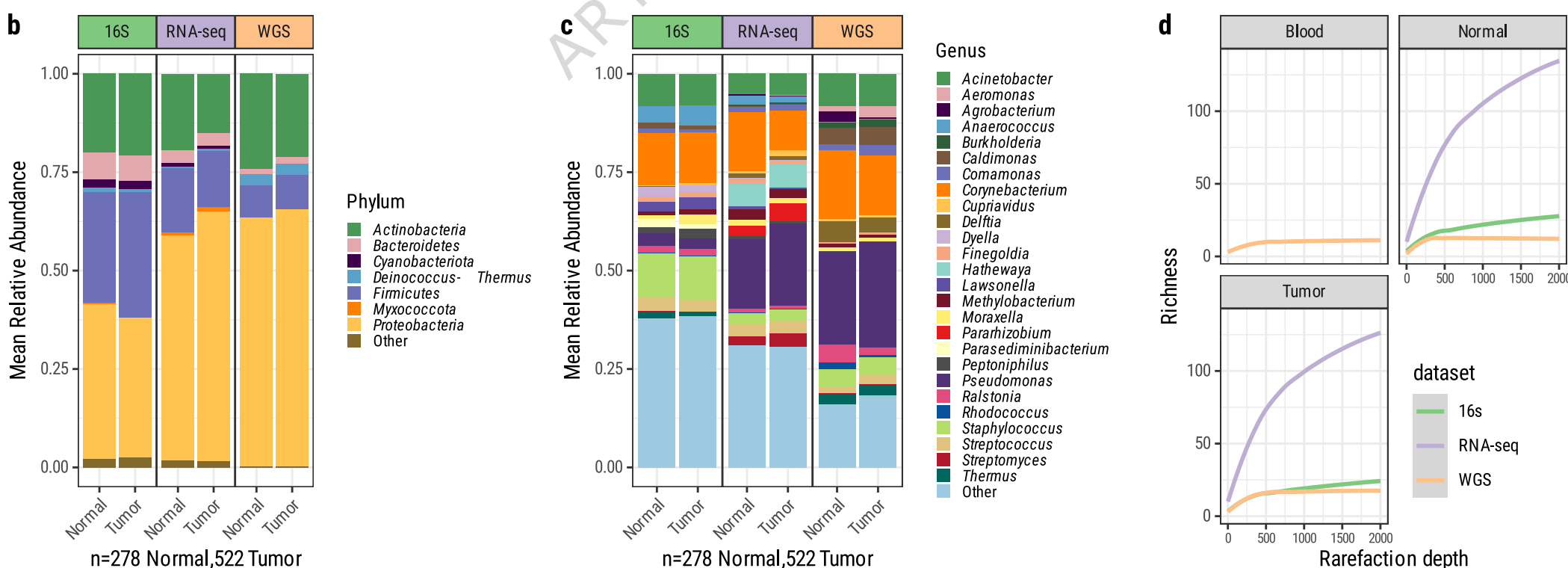
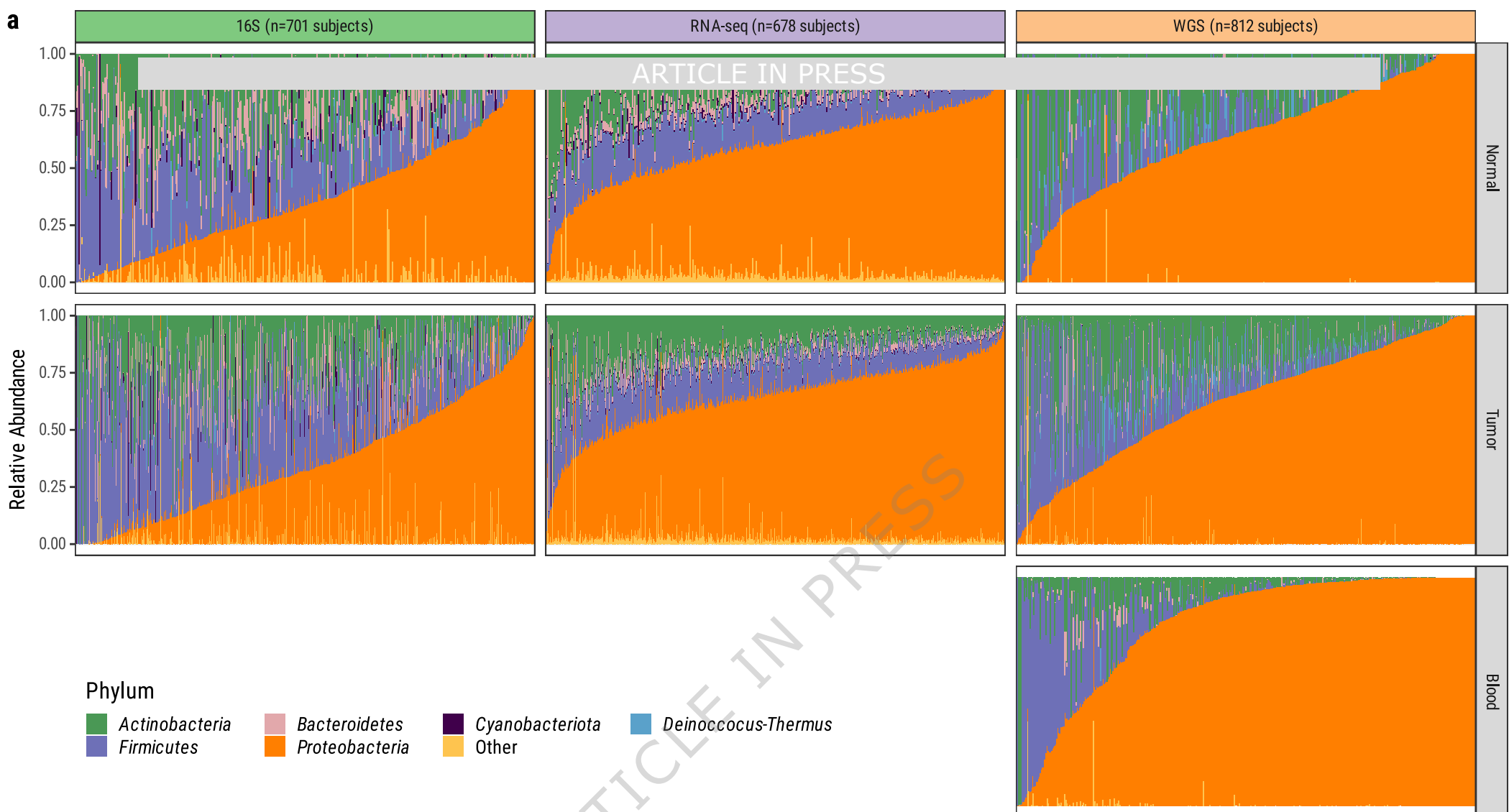
1189 **Figure 3:** Tumor-normal, clinical, and demographic associations with the microbiome. a)  
1190 ANCOM-BC differential abundance results with Holm method for multiple testing correction,  
1191 and b) comparison of Shannon alpha diversity between paired tumor and normal samples using  
1192 genus-level 16S data ( $n=385$  tumor-normal pairs) using a two-sided Wilcoxon test. Boxplot  
1193 centers, upper and lower bounds, and whiskers represent median, upper and lower quartiles,  
1194 and quartiles +/- 1.5 inter-quartile range, respectively. c) ANCOM-BC differential abundance  
1195 results with Holm method multiple testing correction, and d) comparison of Shannon alpha  
1196 diversity between paired tumor and normal samples using genus-level RNA-seq data ( $n=525$   
1197 tumor-normal pairs) using a two-sided Wilcoxon test. Boxplot centers, upper and lower bounds,  
1198 and whiskers represent median, upper and lower quartiles, and quartiles +/- 1.5 inter-quartile  
1199 range, respectively. e) Genus-level alpha diversity and richness in tumors associated via  
1200 generalized linear models with clinical features, adjusted for study site. RNA-seq ( $n=661$ ), 16S  
1201 ( $n=572$ ), and meta-analyzed WGS ( $n=704$ ) samples were rarefied to 500, 250, and 100 bacterial  
1202 reads respectively. Stage I tumors, adenocarcinoma histology, and European (EUR) ancestry  
1203 serve as references. Unadjusted p-values are shown; all tests are non-significant (FDR>0.05)  
1204 after multiple testing correction. Points represent regression coefficient, error bars signify  
1205 standard error. WGS = whole genome sequencing; RNA-seq = RNA sequencing; 16S = 16S rRNA  
1206 gene sequencing; AMR=American; EAS=East Asian.

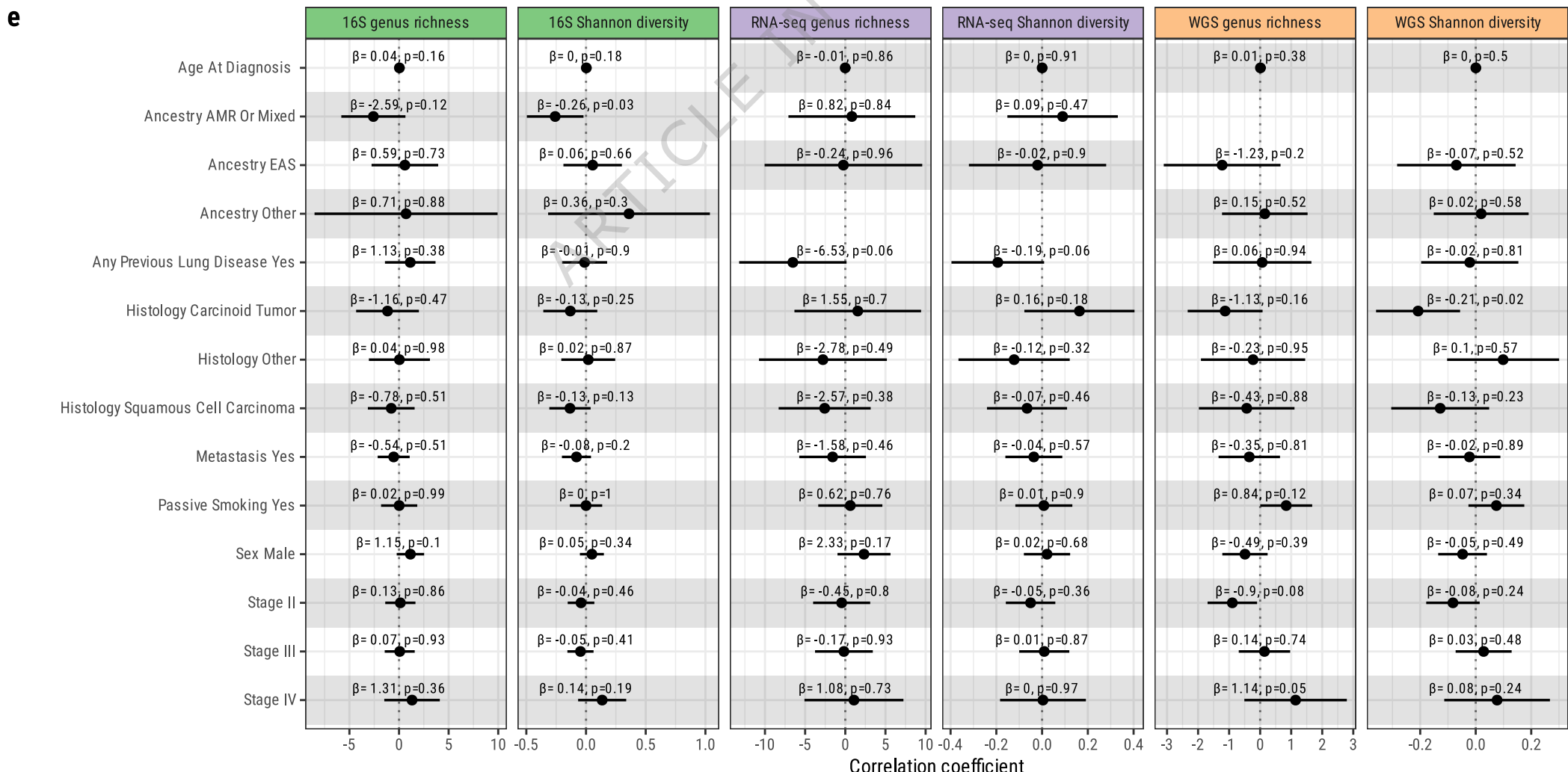
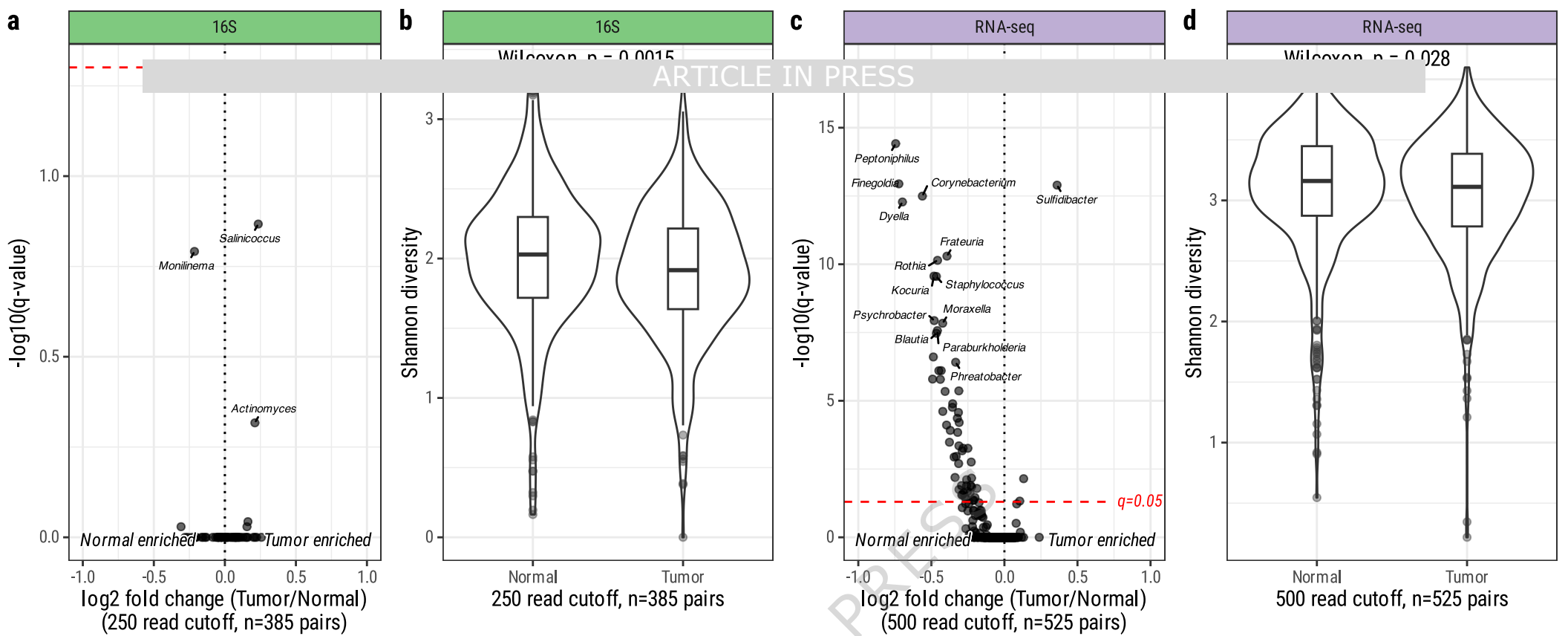
1207

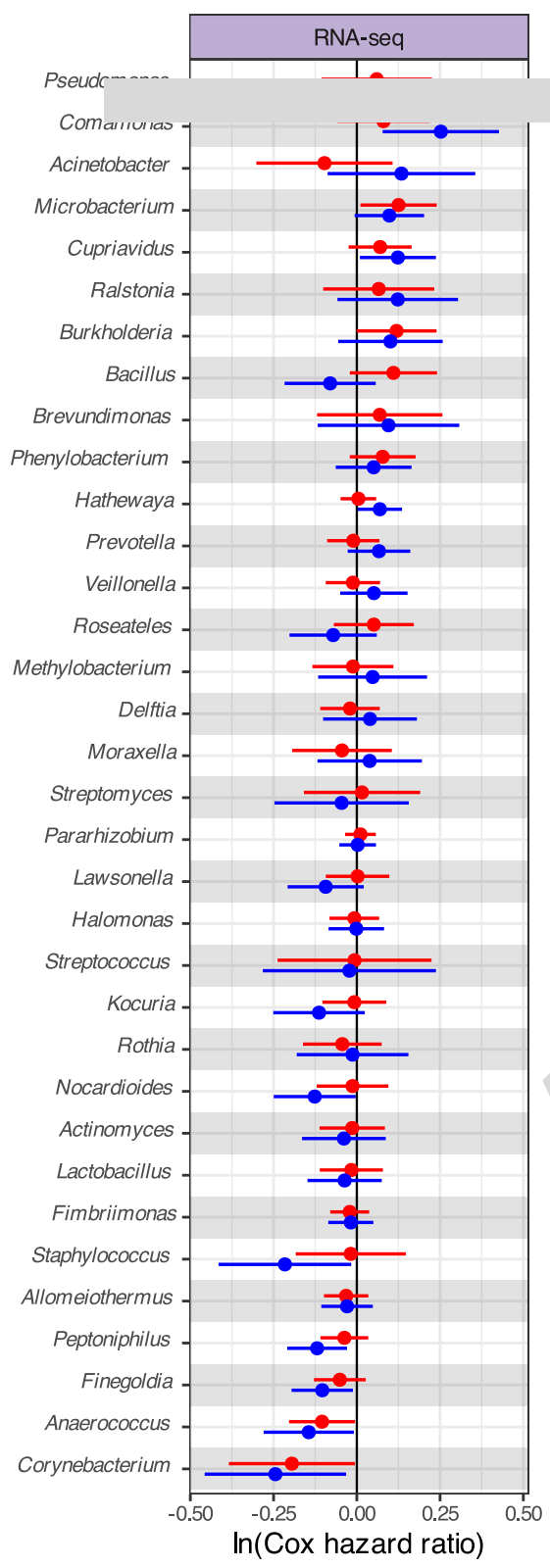
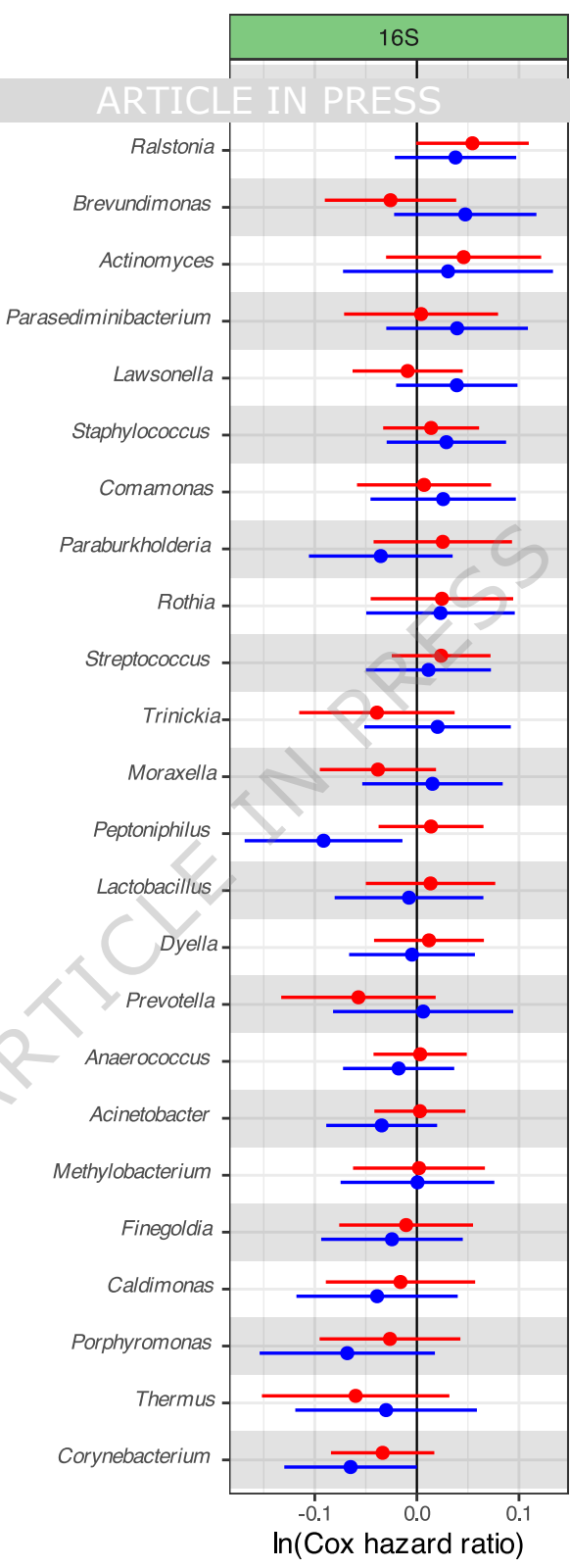
1208 **Figure 4:** Survival associations with individual bacterial taxa. a) Cox proportional hazard model  
1209 of ten-year survival with RNA-seq bacterial relative abundances including genera with minimum  
1210 50 reads in 10% of samples, b) 16S bacterial relative abundances including genera with  
1211 minimum 10 reads in 10% of samples, and c) meta-analyzed WGS bacterial relative abundances  
1212 including genera with minimum 10 reads in 10% of samples. All analyses were stratified by  
1213 study site, age at diagnosis (age>65 or  $\leq 65$ ), and stage (stage I or stages II-IV), and further  
1214 adjusted by histology and age in ten year categories. All associations are not significant  
1215 (FDR>0.05) after multiple testing correction. Points represent log Cox hazard ratio, error bars  
1216 signify standard error. RNA-seq  $n = 587$  tumor samples, 482 normal samples; 16S  $n = 488$  tumor

1217 samples, 395 normal samples; WGS  $n = 647$  tumor samples, 375 blood samples. WGS = whole  
1218 genome sequencing; Rna-seq = RNA sequencing; 16S = 16S rRNA gene sequencing.  
1219  
1220







**a****b****c**